© 2021. Published by The Company of Biologists Ltd | Journal of Cell Science (2021) 134, jcs254359. doi:10.1242/jcs.254359

RESEARCH ARTICLE

Vimentin tunes cell migration on collagen by controlling β1 integrin activation and clustering

Zofia Ostrowska-Podhorodecka[1,*], Isabel Ding[1], Wilson Lee[1], Jelena Tanic[1], Sevil Abbasi[1], Pamma D. Arora[1], Richard S. Liu[1], Alison E. Patteson[2,3], Paul A. Janmey[2] and Christopher A. McCulloch[1]

ABSTRACT

Vimentin is a structural protein that is required for mesenchymal cell migration and directly interacts with actin, β1 integrin and paxillin. We examined how these interactions enable vimentin to regulate cell migration on collagen. In fibroblasts, depletion of vimentin increased talin-dependent activation of β1 integrin by more than 2-fold. Loss of vimentin was associated with reduction of β1 integrin clustering by 50% and inhibition of paxillin recruitment to focal adhesions by more than 60%, which was restored by vimentin expression. This reduction of paxillin was associated with 65% lower Cdc42 activation, a 60% reduction of cell extension formation and a greater than 35% decrease in cell migration on collagen. The activation of PAK1, a downstream effector of Cdc42, was required for vimentin phosphorylation and filament maturation. We propose that vimentin tunes cell migration through collagen by acting as an adaptor protein for focal adhesion proteins, thereby regulating β1 integrin activation, resulting in well-organized, mature integrin clusters.

This article has an associated First Person interview with the first author of the paper.

KEY WORDS: PAK1, Talin, Paxillin, Vimentin, β1 integrin, Cell migration

INTRODUCTION

Epithelial–mesenchymal transition (EMT) is an integral process in embryogenesis, wound healing and discrete pathologies such as organ fibrosis and cancer progression. In EMT, epithelial cells undergo phenotypic and functional modifications that accompany their conversion into mesenchymal cells (Acloque et al., 2009; Kaimori et al., 2007; Lamouille et al., 2014; Nieto, 2009; Shibue and Weinberg, 2017; Thiery et al., 2009; Thiery and Sleeman, 2006). Activation of EMT results in reduction of cytokeratin, increased expression of proteins associated with mesenchymal lineages, such as vimentin, fibronectin and type I collagen (Kaimori et al., 2007; Lamouille et al., 2014; Shibue and Weinberg, 2017), and the conversion to a migratory phenotype in which cells increase their expression of β1 integrins (Liu et al., 2015a). These alterations facilitate the migration of mesenchymal cells through dense collagenous matrices, partly by generating long cell extensions that can intercalate between collagen fibrils (Grinnell et al., 2006). Although vimentin is a marker of fibroblast lineages (Venkov et al., 2007), its role in regulating cell migration through collagen is not well understood. Notably, physical reorganization of fibrillar proteins that accompanies the migration of fibroblasts through extracellular matrices is an important collagen remodeling pathway (Feng et al., 2014) and is crucial for the maintenance of organ health in mammals (Cox and Erler, 2011).

Fibroblast migration through fibronectin and collagen matrices requires the formation of adhesions enriched with β1 integrin (Maemura et al., 1995; Zeltz and Gullberg, 2016), which undergoes activation as a result of allosteric modifications that increase binding affinity (Arjonen et al., 2012). Integrin activation may involve bidirectional processes in which tightly regulated binding of intracellular proteins to integrin cytoplasmic tails and matrix ligand binding to extracellular domains contribute to two-way signaling. One of the regulators of 'inside-out' integrin activation is talin 1, which binds to β-integrin cytoplasmic tails and anchors actin filaments (Calderwood et al., 2013; Wang et al., 2019). Talin binding alters the orientation of the β integrin transmembrane domain. By separating the α- and β-integrin cytoplasmic subunits, talin induces an extended open conformation of integrin extracellular domains (Kim et al., 2011; Klapholz and Brown, 2017; Shattil et al., 2010). In addition, the association of integrin cytoplasmic tails with a broad repertoire of cytoskeletal and signaling proteins facilitates initiation of integrin clustering, which strengthens cell attachment to matrix ligands and provides physical continuity between extracellular matrix and cytoskeletal polymers such as actin filaments (Baade et al., 2019; Liu et al., 2015b; Puklin-Faucher and Sheetz, 2009). As integrins are activated by ligand binding, during initial attachment to the matrix, cells may adhere quite tightly, even in the absence of 'inside-out' integrin activation (Anthis et al., 2009; Tanentzapf and Brown, 2006). High-affinity, talin-binding integrins can form adhesions, but normal cell spreading is only possible with integrins that can recruit the signaling adapter protein paxillin (Pinon et al., 2014).

Talin colocalizes with paxillin near the plasma membrane (Case and Waterman, 2015; Critchley, 2009; Kanchanawong et al., 2010). After initial integrin–extracellular matrix (ECM) engagement and actin reorganization, paxillin contributes to the formation of cell extensions as a result of binding to the Rho GTPases Cdc42 and Rac1 (Hodge and Ridley, 2016; Iden and Collard, 2008; Jaffe and Hall, 2005). One of the downstream effectors of Cdc42 and Rac is the p21-activated kinase 1 (PAK1), which interacts with these small GTPases to regulate the actin assembly required for the formation of cell extensions (Delorme-Walker et al., 2011; Pirruccello et al., 2006; Zhao and Manser, 2012). PAK1 phosphorylates paxillin, which in turn enhances the turnover rate of cell adhesions and regulates leading-edge protrusion and cell migration (Nayal et al., 2006). PAK1 may also regulate the reorganization of vimentin

[1]Faculty of Dentistry, University of Toronto, Toronto, ON M5G 1G6, Canada. [2]Department of Physiology, University of Pennsylvania, Philadelphia, PA 19104-6393, USA. [3]Physics Department, Syracuse University, Syracuse, NY 13244, USA.

*Author for correspondence (zofia.ostrowska.podhorodecka@utoronto.ca)

Z.O.-P., 0000-0002-2261-7488; S.A., 0000-0003-4451-8541; A.E.P., 0000-0002-4004-1734

Handling Editor: Michael Way
Received 15 September 2020; Accepted 20 January 2021

Journal of Cell Science (2021) 134, jcs254359. doi:10.1242/jcs.254359

filaments by phosphorylation, a process that modifies filament assembly and maturation, cell adhesion dynamics and cell extension formation (Eriksson et al., 2004; Goto et al., 2002; Li et al., 2006). Currently it remains obscure how vimentin regulates collagen-dependent migration despite its prominent expression in fibroblasts and localization to cell adhesions (Kim et al., 2010; Kreis et al., 2005; Terriac et al., 2017). We considered that vimentin recruits paxillin into focal adhesions, which enables Cdc42-dependent PAK1 activation and, finally, cell extension formation.

Vimentin intermediate filaments are centrally involved in cell extension formation and migration through fibronectin (Ding et al., 2020). In endothelial cells, migration through collagen matrices may depend on the colocalization of vimentin with the α2β1 integrin, a fibrillar collagen receptor (Kreis et al., 2005). Vimentin localizes to cell–matrix adhesions in a structure-dependent manner: small, nascent adhesions contain small vimentin particles whereas mature, large adhesions contain long filaments (Terriac et al., 2017). The abundance of vimentin and its configuration (e.g. squiggles, protofilaments, filaments) regulate cell adhesion strength and migration (Ding et al., 2020; Helfand et al., 2011). Vimentin interacts with adhesion proteins and may aggregate in adhesion complexes to regulate the focal adhesion formation (Dave et al., 2013; Menko et al., 2014; Terriac et al., 2017; Tsuruta and Jones, 2003). Currently, the mechanisms by which vimentin controls cell adhesion, cell extension formation and migration through soft connective tissues are not defined. Here, we examined whether vimentin acts as an adaptor protein that orchestrates the formation, stabilization and turnover of β1 integrin-dependent cell adhesions to collagen in time and space, which in turn leads to cell extension formation and cell migration.

RESULTS

Vimentin regulates cell extensions in a substrate-dependent manner

As vimentin intermediate filaments are involved in the regulation of cell shape (Lowery et al., 2015; Mendez et al., 2010), formation and stabilization of extensions required for cell migration on fibronectin substrates (Ding et al., 2020), we examined cell extension formation in NIH-3T3 cells (3T3) and mouse embryonic fibroblasts (mEFs) plated for 4 h on monomeric collagen (100 µg/ml) or fibronectin (10 µg/ml). For reduction of vimentin expression, cells were treated with scrambled siRNA (control) or ON-TARGET VIM siRNA 36 h before re-plating on ECM. In addition, we examined Vim null mEFs obtained from vimentin-knockout mice (Patteson et al., 2019) to assess the effects of long-term vimentin deletion on cell extension formation. Immunoblotting showed greater than 90% reduction of vimentin expression after siRNA knockdown (KD; Fig. 1A). Confocal images of vimentin and actin filaments showed that vimentin expression levels strongly affected cell morphology when cells were cultured on collagen, whereas when plated on fibronectin there was only a modest effect on cell morphology (Fig. 1B). Quantification of cell surface area and circularity, as well as numbers and lengths of cell extensions (defined as processes that extended >10 µm from the cell centroid) indicated that vimentin affects cell morphology on collagen but not fibronectin. In cells with reduced vimentin expression (siRNA-treated or null cells), cell surface area on collagen surfaces was reduced by 45% in 3T3 cells and by more than 30% for mEFs compared with that of control cells (Fig. 1C). Furthermore, in cells with vimentin KD, there was a greater than 60% reduction in the number of cell extensions for cells plated on collagen (Fig. 1D). Similarly, when cells were cultured on collagen, the mean length of extensions was reduced (by 30% for 3T3 cells and 50% for mEFs) as a result of vimentin KD or deletion (Fig. 1E). Finally, analyses of morphology showed that loss of vimentin increased cell circularity by 60–70%, but only in cells that were cultured on collagen (Fig. 1F). These data prompted us to examine the relationship between vimentin expression and the formation of extensions in cells plated on collagen.

Loss of vimentin increases collagen-binding receptor activation

As vimentin associates with the α2β1 integrin and is enriched in β1 integrin-containing focal adhesions (Kreis et al., 2005), we assessed whether vimentin affects the expression of collagen adhesion receptors normally expressed in mesenchymal cells, specifically the β1 integrin and DDR2. Besides β3 and β7 integrins, the β1 is also a common integrin subunit in fibronectin receptors (Liao et al., 2002; Pankov and Yamada, 2002). Evaluation of whole-cell lysates showed that vimentin KD increased the level of β1 integrin but with no effect on DDR2 protein expression (Fig. 2A). We examined by flow cytometry the abundance of total membrane-associated and activated β1 integrin at the plasma membrane in non-permeabilized cells. Short-term vimentin KD by siRNA did not affect β1 integrin expression, whereas repeated passaging (*n* passages>10) of vimentin null mEFs resulted in a slight increase (∼20%) in β1 integrin compared with levels in the control (Fig. 2B). With a separate approach for estimating β1 integrin activation, we analyzed the binding of fibrillar collagen-coated 2 µm beads after 2 h incubation with cells. Flow cytometry showed that loss of vimentin increased collagen-coated bead binding by 40% for 3T3 cells, 170% for vimentin-null mEFs and 68% for vimentin siRNA mEFs (Fig. 2C). When the same analyses were performed with fibronectin beads, there were no substantial differences in β1 integrin activation and binding between wild-type (WT) and vimentin-null cells (Fig. S1A,B). Moreover, the addition of 0.2 mM $MnCl_2$ to activate integrins did not affect fibronectin-coated bead binding in WT mEFs, whereas in vimentin-null cells, fibronectin-coated beads were bound with the same efficiency as collagen-coated beads (Fig. S1C). Surprisingly, the addition of fibronectin-coated beads to WT and vimentin-null mEFs cultured on fibronectin-coated surfaces resulted in a 2-fold increase in bead binding by vimentin-null mEFs (Fig. S1D). These results were affected by increasing ligand accessibility (examined in a receptor abundance assay, Fig. 2B), which indicated increased capacity for ligand binding by receptors. We also measured β1 integrin activation with a neo-epitope antibody (clone 9EG7; Lenter et al., 1993). For cells plated on collagen, vimentin KD was associated with a 2-fold increase in β1 integrin activation in 3T3 cells (treated with siRNA), a 9-fold increase in vimentin-null mEFs and a 7-fold increase in mEFs treated with siRNA, compared with activity in their respective siRNA control or WT controls (Fig. 2D). The fluorescence intensity of β1 integrin receptors assessed by microscopy (Fig. 2E) was consistent with flow cytometry data.

We also measured adhesion strength using beads coated with fibrillar collagen (1 mg/ml) and a shear force assay (3.5 Pa) (Chong et al., 2007). Quantification of bead binding after repeated washes showed that loss of vimentin increased collagen binding strength of 3T3 cells by more than 64% (Fig. 2F) and of mEFs treated with vimentin siRNA by more than 33% (Fig. 2G). These differences in binding strength disappeared after large numbers of washes (>8). Analysis of vimentin-null mEFs showed consistently stronger collagen binding, which was not dependent on the number of washes. In contrast, KD of vimentin with siRNA reduced the relative binding strength of cells incubated with fibronectin-coated

Journal of Cell Science (2021) 134, jcs254359. doi:10.1242/jcs.254359

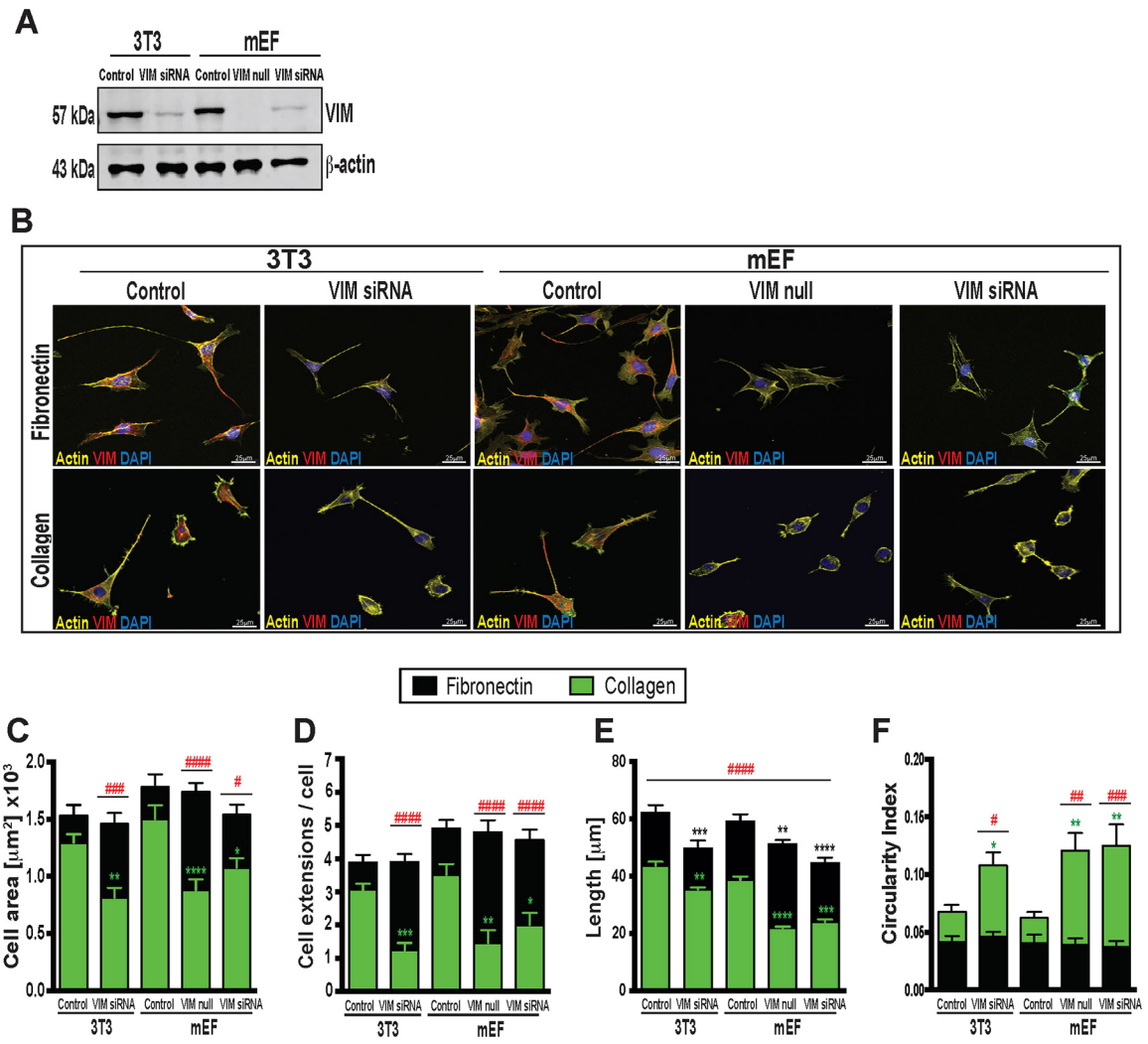

Fig. 1. Vimentin expression affects cell morphology in a substrate-dependent manner. (A) Vimentin (VIM) immunoblot for 3T3 and mouse embryonic fibroblasts (mEF). Wild-type cells were treated with scrambled siRNA (control) or ON-TARGET vimentin siRNA (VIM siRNA). mEF vimentin-null (VIM null) cells were derived from vimentin-null mice. β-actin was used as a loading control. (B) Representative confocal images of 3T3 and mEF cells cultured on fibronectin or monomeric collagen for 4 h. Cells were triple-stained with antibodies against vimentin (red), Rhodamine–phalloidin for actin (yellow) and DAPI (blue). Scale bars: 25 µm. (C–F) Quantification of cell morphology parameters for cells plated on fibronectin (black) or collagen (green). Bar charts show mean cell area (C), number of extensions per cell (D), length of cell extensions (E) and the circularity index (F). Cells were quantified using ImageJ (n=3, 45 cells per group). Data are shown as mean±s.e.m. *P<0.05, **P<0.01, ***P<0.001, ****P<0.0001 compared with control. $^{\#}P$<0.05, $^{\#\#}P$<0.01, $^{\#\#\#}P$<0.001, $^{\#\#\#\#}P$<0.0001 between measurements of cells on fibronectin and cells on collagen (two-way ANOVA test used).

(10 µg/ml) fluorescent beads (23% reduction for 3T3 cells and 49% reduction for mEFs), whereas vimentin deletion in mEFs reduced binding strength of fibronectin-coated beads by 14% (Fig. S1E,F). Notably, exposing cells to increased fibronectin by adding fibronectin-coated beads to cells cultured on fibronectin-coated dishes, resulted in slightly stronger bead binding by vimentin-null mEFs (Fig. S1G).

We assessed whether collagen bead binding was indeed dependent on the β1 integrin with the use of an inhibitory antibody (Lenter et al., 1993). Quantification of bead binding showed that inhibition of the β1 integrin blocked the increase of binding strength caused by vimentin depletion (Fig. 2H). For assessing the specificity of vimentin-mediated activation of the β1 integrin, we examined fibrinogen-coated bead binding, which is dependent on β2 and β3 integrin receptors (Hantgan et al., 2010) but not the β1 integrin. We found that vimentin depletion decreased initial fibrinogen binding strength (Fig. 2I), indicating that vimentin plays a role in the regulation of β1, but not in β3 integrin activation. Furthermore, negative controls that utilized poly-L-lysine-, fibrinogen- and BSA-coated fluorescent beads also showed no differences in binding after vimentin depletion (Fig. S1H). These data support the notion that vimentin plays a role in regulating integrin function activation or inhibition depending on the access of the β1 integrin to collagen or fibronectin, respectively.

Vimentin affects the clustering and spatial distribution of the β1 integrin on collagen

As cell binding to certain matrix ligands (e.g. collagen) is associated with β1 integrin activation and clustering (Welf et al., 2012), we examined the spatial distribution of activated β1 integrins. We found that the level of vimentin expression was associated with alteration of activated β1 integrins in focal adhesions (Fig. 3A). In cells with vimentin KD, the size of β1 integrin clusters was reduced by 60% in 3T3 cells and 50% in mEFs cultured on collagen. Re-expression of

Journal of Cell Science (2021) 134, jcs254359. doi:10.1242/jcs.254359

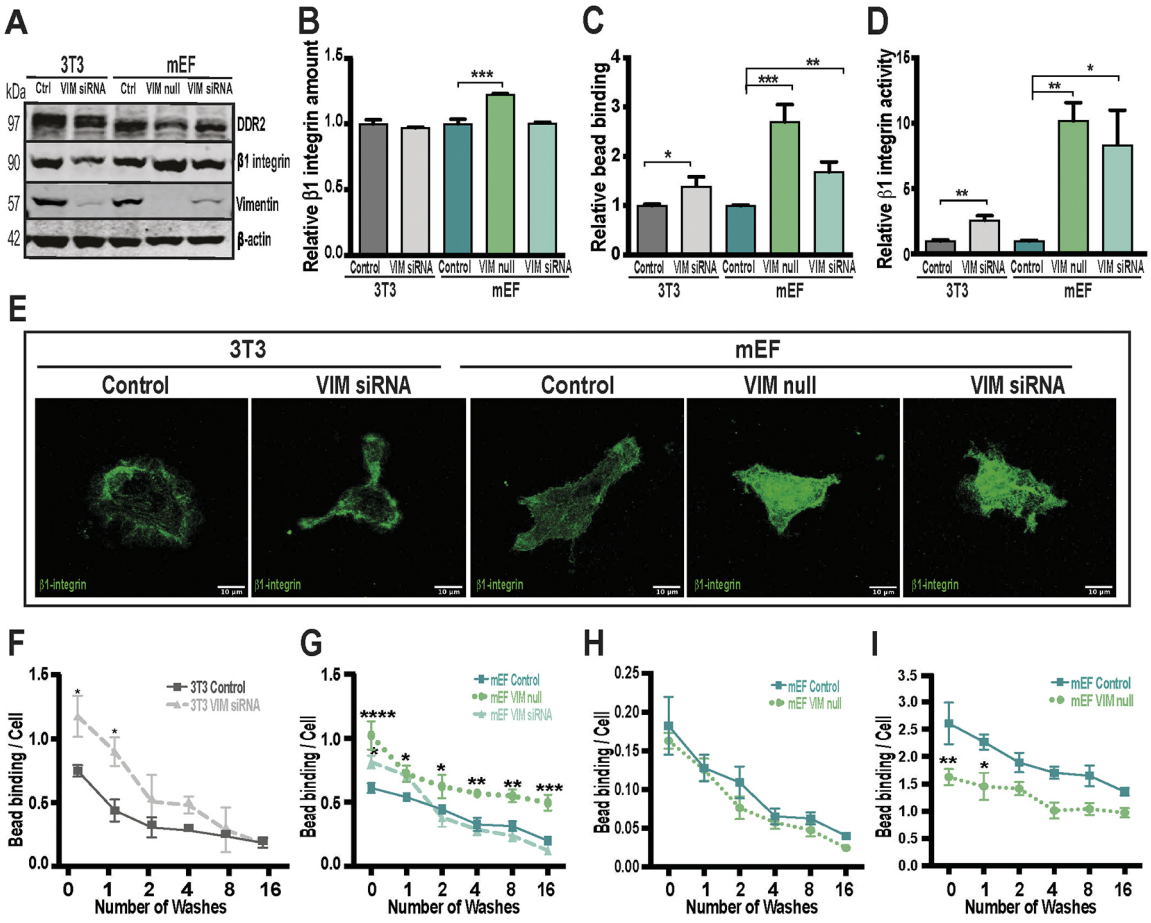

Fig. 2. Vimentin level determines β1 integrin activation and cell adhesion to collagen. (A) Wild-type 3T3 and mEF cells treated with control siRNA (control) or vimentin siRNA (VIM siRNA), as well as vimentin-null mEF cells (VIM null), were cultured on monomeric collagen. Whole-cell lysates were immunoblotted for β1 integrin subunit, DDR2, vimentin and β-actin with appropriate antibodies. (B) Quantification of the relative abundance of membrane-associated β1 integrin by flow cytometry. 3T3 control (dark gray) and VIM siRNA (light gray) cells, and mEF control (teal), VIM null (green) and VIM siRNA (turquoise) cells were immunostained with the KMI6 clone antibody. (C) Relative recruitment of collagen-coated 2 µm fluorescent beads for all indicated cell types from flow cytometry analyses. (D) Estimation of relative β1 integrin activation after 3 h incubation on collagen. Cells were immunostained for β1 integrin using 9EG7 clone antibody, which recognizes an activation epitope in the β1 integrin chain. Data in B–D are mean±s.e.m.; *n*=3, 10,000 cells. (E) Confocal images of 3T3 (control and VIM siRNA) and mEF (control, VIM null and VIM siRNA) cells on collagen and immunostained for β1 integrin with 9EG7 clone antibody. Scale bars: 10 µm. (F,G) Relative binding strength of control cells (square, solid line) and vimentin-deficient (VIM siRNA, triangle, dashed line; VIM null, circle, dotted line) 3T3 (F) and mEF (G) cells. Fluorescent beads (2 µm) were coated with 1 mg/ml fibrillar collagen and incubated with cells (8 beads/cell) for 2 h. Cells with bound beads were subjected to 0, 1, 2, 4, 8 and 16 washes. Plots represent the number of bound beads per cell after each wash. (H,I) Relative binding strength of mEF WT (mEF control) and VIM null cells to collagen-coated fluorescent beads after inhibition of β1 integrin activation (H) and fibrinogen-coated (1 mg/ml) 2 µm fluorescent beads (I). Data in F–I are mean±s.e.m.; *n*=3, 2500 cells. All quantifications are derived from three independent experiments. **P*<0.05, ***P*<0.01, ****P*<0.001, *****P*<0.0001 compared with control cells (two-way ANOVA tests used).

vimentin in vimentin-null mEFs (Fig. S2A) restored the size of β1 integrin clusters by 42% (Fig. 3B). Contemporaneously, there was a greater than 55% increase in the number of small (~0.5 µm) β1 integrin clusters after vimentin depletion for all cell types that were cultured on collagen. After vimentin rescue, there were only 11% more clusters compared with the clusters in control cells (Fig. 3C). Furthermore, measurements of the spatial distribution of β1 integrin clusters with respect to the leading edge of the cell showed that loss of vimentin was associated with a 68% reduction of the size of integrin clusters that formed within 1.75 µm of the leading edge of the cell. Moreover, in mEF vimentin-null cells in which vimentin expression was restored (rescue) showed only 17% smaller clusters compared with those in WT cells. We found no differences for β1 integrin clusters that formed at the cell periphery (i.e. <1.75 µm from the leading edge; Fig. 3D). Under identical experimental conditions, cells cultured on fibronectin-coated surfaces showed no differences in the spatial distribution of β1 integrin clusters or cluster size between WT and vimentin-null mEFs (Fig. S2B–D). Further analysis by confocal imaging of cells plated on fibronectin- or collagen-coated surfaces for 3 h and stained with anti-total (non-activation specific) β1 antibody (clone KMI6; Fig. S2E–G) showed marked similarities to data on integrin activation and clustering obtained with the 9EG7 antibody. Finally, we examined the spatial relationship of β1 integrin cluster size with the number of clusters using Pearson correlation (Fig. 3E). These analyses showed that the size of integrin clusters was negatively correlated with numbers of clusters per cell ($r<-0.5$), which was 3-fold greater for all vimentin-deficient cells: 3T3 siRNA ($P<0.04$), mEF null ($P<0.02$) and mEF siRNA ($P<0.03$). Collectively these results indicate that vimentin affects β1 integrin cluster growth and maturation of focal adhesions. We conclude that vimentin filaments are involved in linking collagen-dependent β1 integrin activation with cluster formation.

Journal of Cell Science (2021) 134, jcs254359. doi:10.1242/jcs.254359

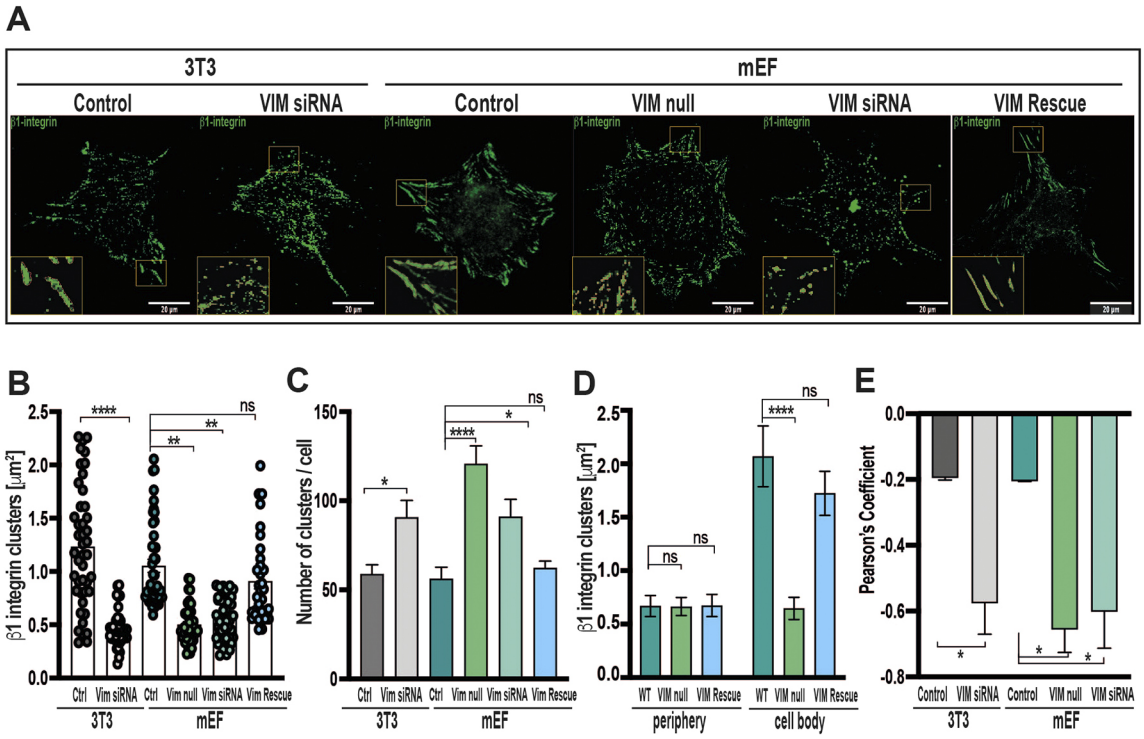

Fig. 3. Vimentin regulates clustering and distribution of β1 integrin. (A) Confocal images of 3T3 cells treated with control siRNA (control) or vimentin siRNA (VIM siRNA), WT mEF cells treated with control or VIM siRNA, vimentin-null mEF cells (VIM null) and VIM null cells expressing vimentin–GFP (VIM rescue) after 3 h on collagen to enable the initiation of cell extension. Cells were immunostained with 9EG7 antibody to estimate the activated fraction of β1 integrin (green). Boxes mark the regions of β1 integrin clusters that were analyzed, shown as higher magnification insets (bottom left). Scale bars: 20 µm. (B,C) Control (Ctrl, dark gray) and VIM siRNA (light gray) 3T3 cells, as well as control (teal), Vim null (green), Vim siRNA (turquoise) and Vim rescue (blue) mEF cells were analyzed for (B) β1 integrin cluster size and (C) β1 integrin cluster number per cell. (D) Distribution of β1 integrin with respect to the leading edge. Cells were quantified using Fiji with a macro for separating the area 1.75 µm from the leading edge and the cell body. WT (teal), VIM null (green) and VIM rescue (blue) mEF cells were plated on collagen for 3 h, fixed and stained for the active subpopulation of β1 integrin and cell membrane (CellBrite). (E) Pearson coefficients of correlation between the size and number of β1 integrin clusters were obtained for the indicated cell lines by quantification of fluorescence images using the Fiji JACoP plugin. Data in B–E are mean±s.e.m. (n=3, 50 cells per group).*P<0.05; **P<0.01; ****P<0.0001; ns, not significant [ordinary one-way ANOVA (B, C) and two-way ANOVA (D) test used].

Vimentin regulates recruitment of cell adhesion complex proteins

The interactions of cell surface integrins with matrix ligands result in integrin clustering and the formation of nascent cell–ECM adhesion structures, such as focal complexes (Geiger et al., 2001). Focal complexes are dynamic protein aggregates that mature into more stable, larger structures (focal adhesions) that form mechanical links between actin filaments and the ECM (Kanchanawong et al., 2010). As vimentin regulates the lifetime, stability and maturation of focal adhesions (Burgstaller et al., 2010), we considered that vimentin may also affect the assembly and function of adhesion-associated molecules in time and space, which in turn may regulate β1 integrin activation. Accordingly, we looked for a link between vimentin expression and quantitative changes in the abundance of proteins in adhesion complexes by quantitative tandem mass spectroscopy. Initial mass spectrometry analyses of collagen bead-associated proteins were used to examine protein abundance ratios for vimentin-null versus WT mEFs. These data showed that after vimentin depletion, there was ∼2.5-fold more talin 1 in collagen adhesions than in those of WT cells (Fig. S3A). Notably, talin regulates β1 integrin activation (Calderwood et al., 2013). Validation of the mass spectrometry data by immunoblotting showed that vimentin depletion increased talin abundance in collagen-bead associated proteins but did not affect whole-cell talin expression levels (Fig. 4A). The total abundance of β1 integrin, as determined by immunoblotting, was higher in vimentin-null mEFs than WT mEFs, which was consistent with flow cytometry analyses (Fig. 2B). However, the same amount of bound integrins was detected in mEF WT and vimentin-null cells for collagen-associated proteins. Finally, we noticed a loss of paxillin in the collagen bead-associated proteins, suggesting that vimentin may affect the recruitment of paxillin to the focal adhesion complex. This loss of paxillin in the focal adhesions was not explained by a global alteration of expression, because loss of vimentin did not change the total expression of talin, α-actinin, paxillin or PAK1 (Fig. 4A,B; Fig. S3B–E).

As previous data suggest that vimentin filaments of cells involved in healing are linked to paxillin-rich focal adhesions (Menko et al., 2014), we examined whether vimentin may directly interact with paxillin during cell migration. Notably, immunoprecipitation data showed an association between vimentin and paxillin (Fig. 4C). Furthermore, we analyzed whether vimentin depletion leads to alterations of the size or number of paxillin-containing focal adhesions. Confocal images (Fig. 4D) showed that after vimentin depletion, the mean area of focal adhesions was reduced by 44% compared with those of WT cells. In addition, the size of focal adhesions was restored by 22% after vimentin re-expression (Fig. 4E). Moreover, our analyses showed that loss of vimentin increased the number of focal adhesions per cell by more than 2-fold (Fig. 4F), which is an indication of less-mature focal adhesions.

One of the most abundant paxillin-associated proteins in focal adhesions is talin1, which is critical for focal adhesion assembly

Journal of Cell Science (2021) 134, jcs254359. doi:10.1242/jcs.254359

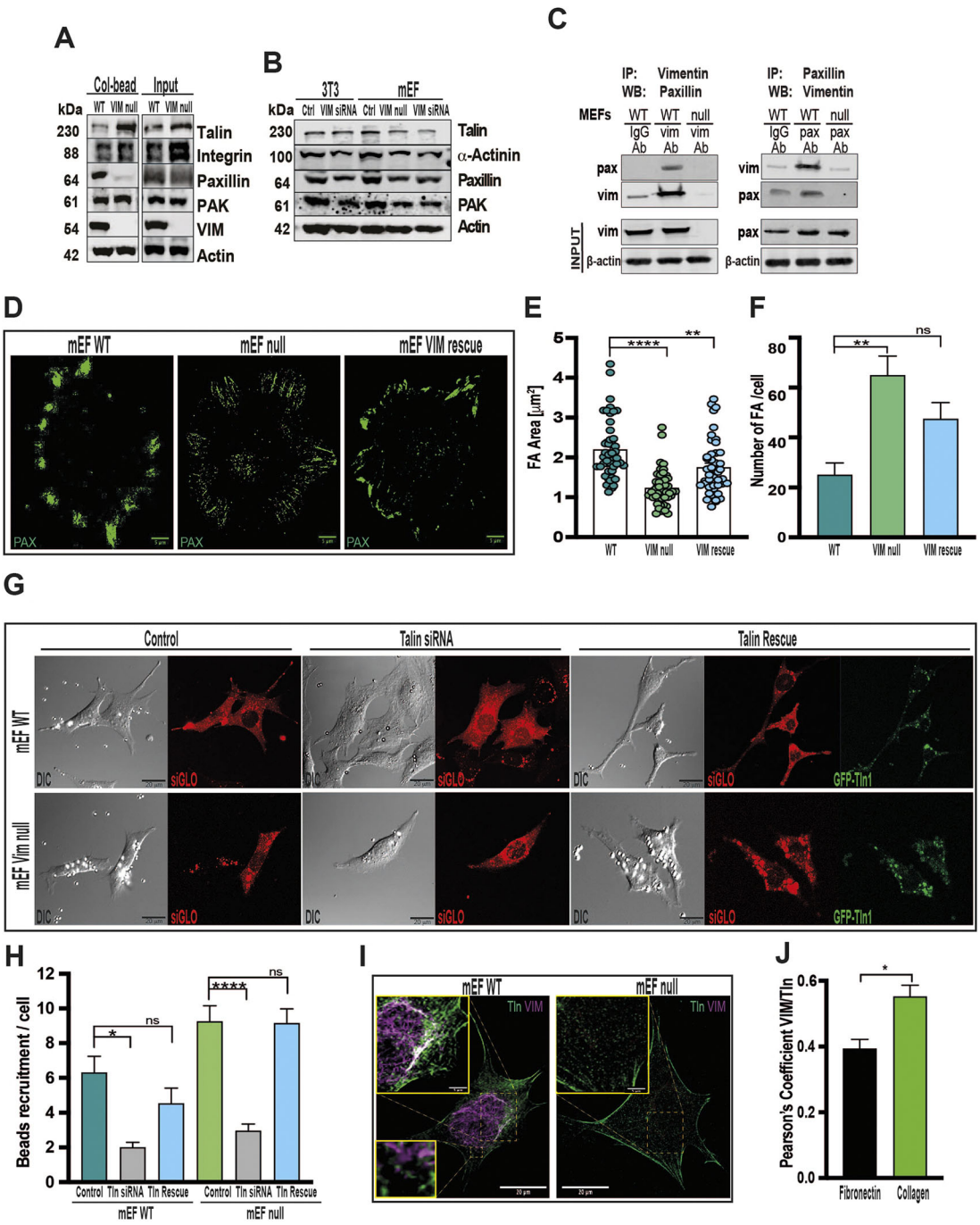

Fig. 4. Vimentin regulates recruitment of cell adhesion complex proteins. (A) Immunoblot of collagen bead-associated focal adhesion proteins (col-bead) and whole-cell lysate (input) for mEF WT and vimentin (VIM)-null cells. (B) Western blot of whole-cell lysates of 3T3 and mEF cells (control siRNA-treated, Ctrl; vimentin siRNA-treated, VIM siRNA; vimentin-null, VIM null) cultured on collagen coated-surfaces were immunostained for talin, α-actinin, paxillin, PAK1 and β-actin (loading control). (C) Vimentin (vim) and paxillin (pax) immunoprecipitation (IP) in WT and vimentin-null mEFs. Left: immunoprecipitation of vim was immunoblotted (WB) for pax and vim. An isotype control antibody (IgG) was used as the immunoprecipitation negative control. Bottom rows show input for vim immunoblot and β-actin loading control. Right, immunoprecipitation of pax was immunoblotted for vim. An isotype control antibody (IgG) was used as the immunoprecipitation negative control. Bottom rows show input pax immunoblot and β-actin loading control. The BCA assay was done for all of the samples, and 140 µg of proteins were loaded per well. (D) Confocal images of focal adhesions were obtained with Zeiss LSM 800 microscope. WT, vimentin-null and vimentin-rescue cells were stained with anti-paxillin antibody (green). Scale bars: 5 µm. (E) Quantification of focal adhesion size (μm^2) and (F) number per cell. mEF WT (teal), mEF vimentin-null (green) and mEF vimentin-rescue cells (blue) were plated on collagen for 3 h. All quantifications are from at least three experiments, 50 cells per group. $^{**}P<0.01$; $^{****}P<0.0001$; ns, not significant (ordinary one-way ANOVA test used). (G) Representative transmitted light (DIC) and confocal images of mEF WT and mEF vimentin-null cells treated with control siRNA, talin siRNA, or talin siRNA and talin1–GFP plasmid (talin rescue, green). Cells were transfected with siGLO (red). Scale bars: 20 µm. (H) Collagen-coated bead recruitment by mEF WT and vimentin-null cells treated with control siRNA (teal), talin (Tln) siRNA (gray), or talin siRNA and talin1–GFP plasmid (Tln rescue, blue). $^{*}P<0.05$; $^{****}P<0.0001$; ns, not significant (two-way ANOVA test used). (I) Olympus SpinSR10 spinning-disk super-resolution microscope images of vimentin (magenta) and talin (green) colocalization in mEF WT and vimentin-null cells. Dashed boxes mark regions shown in inset images. Scale bars: 20 µm, 5 µm (insets). (J) Pearson coefficients of vimentin and talin colocalization obtained by quantification of the fluorescence images of mEF WT cells plated on fibronectin (black) and collagen (green) using the Fiji JACoP plugin. $^{*}P<0.02$ (unpaired *t*-test used). All quantitative data are reported as mean±s.e.m., $n=3$.

Journal of Cell Science (2021) 134, jcs254359. doi:10.1242/jcs.254359

(Dong et al., 2016). Accordingly, we investigated whether talin is involved in the mechanism by which vimentin regulates cell binding to collagen. We examined binding of collagen-coated 2 µm beads in vimentin-WT and -null mEFs after talin deletion and re-expression (Fig. 4G; Fig. S3F). The data showed that after 2 h of incubation with beads, loss of talin reduced bead binding by 68% in WT and vimentin-null mEFs. Talin re-expression resulted in 55% and almost complete restoration of collagen-coated bead binding for WT and vimentin-null cells, respectively, compared with binding by the corresponding control cells (Fig. 4H). Furthermore, high-resolution, sub-diffraction imaging of WT and vimentin-null mEFs (Fig. 4I) indicated that vimentin filaments colocalize with talin (Pearson coefficient, r=0.55; Fig. 4I, upper inset). Small, nonfilamentous vimentin particles were in close proximity with talin, but no colocalization was detected (Fig. 4I, lower inset). Comparisons between cells plated on fibronectin and collagen showed that the colocalization of vimentin and talin was stronger on collagen than on fibronectin ($P< 0.02$; Fig. 4J), suggesting that vimentin may participate in talin-dependent β1 integrin activation.

Vimentin expression regulates cell extension formation by controlling Cdc42 activation

Focal adhesions link and transduce bidirectional forces and signals between the actin cytoskeleton and ECM polymers like collagen. The assembly of focal adhesions requires the activity of Rho GTPases, including RhoA and Cdc42 (Hall, 2005), which promote cell extension formation and cell migration through PAK1 (Hodge and Ridley, 2016; Zhao and Manser, 2012). Accordingly, we investigated whether vimentin depletion interferes with cell extension formation through alterations of Cdc42 activation. Cells were plated on collagen for 3 h, lysed and fractionated, and the resulting supernatants were incubated with PDB–sepharose beads to assess the relative abundance of active Cdc42. Loss of vimentin decreased Cdc42 activation by 65–70% for all types of vimentin-deficient cells (Fig. 5A). We assessed whether vimentin depletion affected other Rho proteins by analyzing Rac1 activity. Depletion of vimentin was associated with a 94% reduction of Rac1 activity; the activity was restored to 57% of the control level after vimentin re-expression (Fig. 5B). We also investigated paxillin-dependent Cdc42 activation by transfecting cells with paxillin siRNA and with a GFP–paxillin expression plasmid that was not affected by the paxillin siRNA we used (Fig. S4A). Paxillin KD in WT cells was associated with 97% reduction of Cdc42 activity; this was restored to 50% of control after paxillin re-expression. Analysis of vimentin-null mEFs showed similar (91%) reduction of Cdc42 activity compared with activity in control cells. Paxillin rescue of these vimentin-null mEFs restored Cdc42 activity by 24% (Fig. 5C). Paxillin silencing resulted in substantial differences in cell morphology (Fig. S4C–E) and the abundance of β1 integrin clusters (Fig. S4H,I) in cells plated on collagen but not on fibronectin. These data indicate that vimentin and paxillin have a substantial impact on Cdc42 activation.

As the active form of Cdc42 is necessary for PAK1 activation through autophosphorylation (Rane and Minden, 2014), we examined how loss of vimentin may affect PAK1 activity by assessing PAK1 phosphorylation levels (Fig. 5D). We found that PAK1 phosphorylation after vimentin depletion was indeed reduced (S141 phosphorylation by 35% and T423 phosphorylation by 24%). As an additional control for PAK1-mediated phosphorylation of vimentin, we used the Cdc42 inhibitor ML141 (10 µM), which showed that inhibition of Cdc42 reduced phosphorylation of PAK S141 in WT mEFs by more than 30% (Fig. 5E; Fig. S4B). No significant changes were found in PAK phosphorylation in vimentin-null mEFs. Finally, we analyzed the effect of Cdc42 inhibition on morphology and focal adhesions in vimentin-WT and -null mEFs with ML141. Confocal images (Fig. S4C) and their quantification showed that inhibition of Cdc42 did not mimic all of the morphological changes (Fig. S4D,E) and focal adhesion effects (Fig. S4F–I) that were observed in vimentin-null cells plated on fibronectin. In contrast, collective measures of cell morphology (Fig. S4D,E) and focal adhesions (Fig. S4F–I) showed that ML141 treatment phenocopied the morphological differences observed in WT and vimentin-null mEFs cultured on collagen.

As Cdc42 plays a central role in cell extension formation, we evaluated cell extension formation by immunostaining for the filopodia tip marker myosin-10 (Fig. 5F). These data showed that vimentin depletion was associated with reduced cell extension formation (>56%; Fig. S4J). Wound healing assays in cultured cells treated with scrambled siRNA (control) or with vimentin siRNA and then plated on collagen, showed visually evident differences in the rate of gap closure after vimentin KD. Time-lapse images of *in vitro* wound closure showed that loss of vimentin delayed wound healing (Fig. 5G). Furthermore, we found no differences in cell migration of vimentin-WT and -null mEFs plated on fibronectin (Fig. S4K). Estimates of migration velocity (Fig. 5H) showed that compared with controls, vimentin KD decreased migration velocity by 36% for 3T3 cells and by more than 35% for mEFs. Collectively these data indicate that vimentin affects the PAK1 activation pathway through inhibition of paxillin-related Cdc42 activation, which in turn contributes to the regulation of cell extension formation and regulation of focal adhesion size in collagen-dependent manner.

Vimentin phosphorylation is involved in the formation of cell extensions

During filament assembly, vimentin undergoes several posttranslational modifications (Shi et al., 2016; Snider and Omary, 2014) including phosphorylation, which affects filament assembly and maturation (Eriksson et al., 2004). PAK1 mediates vimentin phosphorylation at S38, S56 and S72 (Ding et al., 2020; Eriksson et al., 2004; Goto et al., 2002; Li et al., 2006) but it is not known whether vimentin phosphorylation regulates β1 integrin-dependent formation of focal adhesions and cell extensions. We first examined vimentin phosphorylation in 3T3 and mEF cells that had been plated for 3 h on collagen-coated surfaces. To evaluate whether inhibition of PAK1-dependent vimentin phosphorylation is involved in β1 integrin activation and cell extension formation, we used IPA3, a PAK-specific inhibitor (Rudolph et al., 2013). Immunoblot with phospho-vimentin antibodies (Fig. 6A) indicated that IPA3 treatment reduced PAK1-dependent vimentin S39, S56 and S71 phosphorylation by 40%, 60% and 20%, respectively, for 3T3 cells. Similarly, there were 45–67% reductions of vimentin phosphorylation in mEFs (Fig. 6B). Immunostaining for vimentin showed that IPA3 treatment caused spatial reorganization of vimentin filaments, which included vimentin aggregation around the nuclei (Fig. 6C). Quantification of extensions showed that IPA3 treatment and inhibition of vimentin phosphorylation was associated with a greater than 70% reduction of the number of extensions (Fig. 6D). Furthermore, the length of extensions in IPA3-treated cells was reduced by 70%, compared with those of vehicle-treated control cells (Fig. 6E). As IPA3 may affect PAK kinases other than PAK1 (Deacon et al., 2008), we examined cells in which mutant PAK1 was expressed. In these experiments, similar results as those obtained with IPA3 were found for vimentin filament reorganization (Fig. 6F) and

Journal of Cell Science (2021) 134, jcs254359. doi:10.1242/jcs.254359

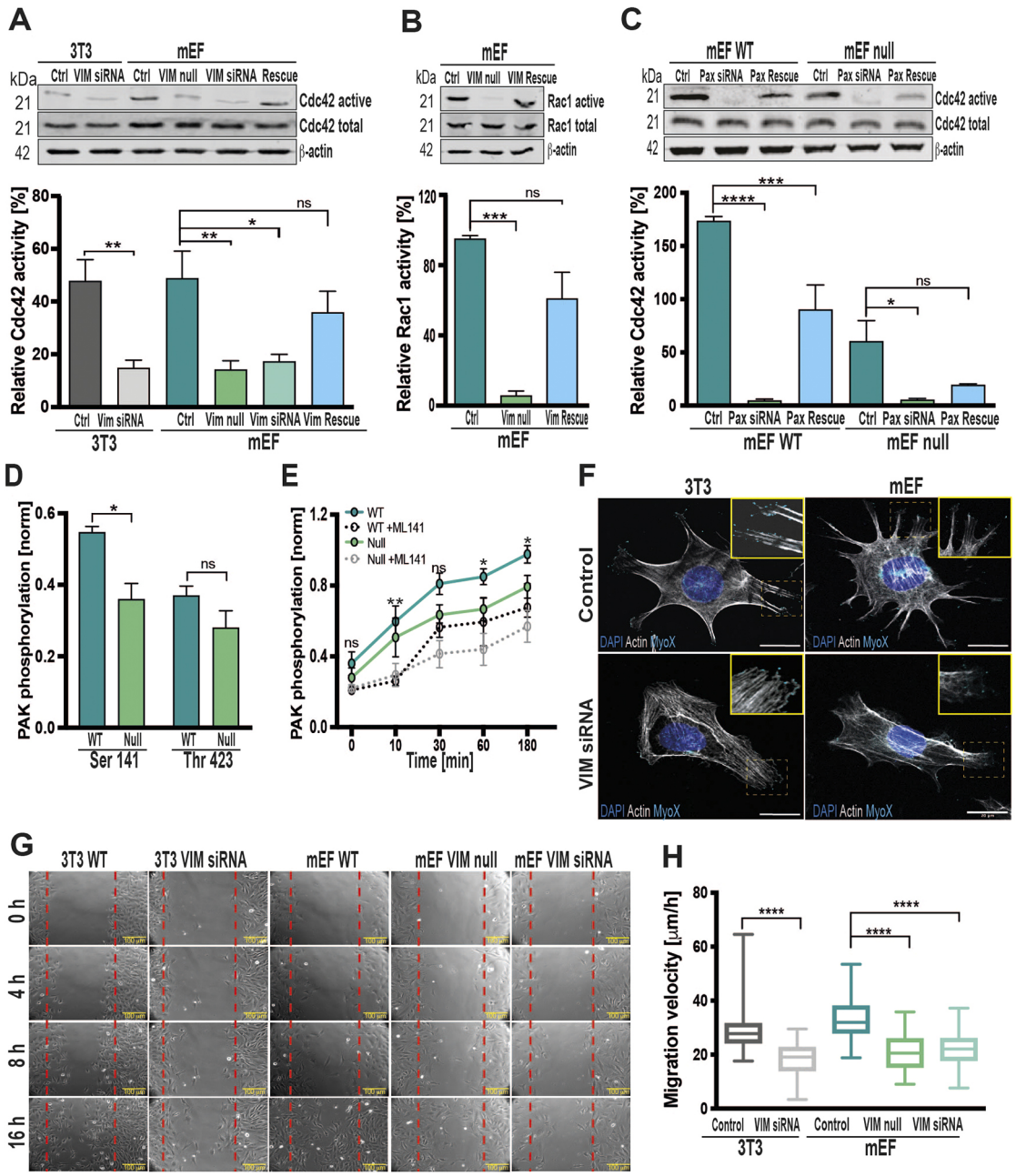

Fig. 5. Effects of vimentin deletion on Cdc42 activation and filopodia formation. (A) Cells were cultured for 3 h on collagen-coated 100 mm dishes, lysed and fractionated into supernatants and pellets. Supernatants were incubated with PDB–sepharose beads overnight, separated by SDS–PAGE and immunoblotted with specific antibodies against Cdc42 and β-actin. Upper panel shows an activated fraction of Cdc42 bound to PDB-beads. Middle panel represents the total amount of Cdc42 in cell lysate. The lower panel shows β-actin loading control. Quantification of the relative activation of Cdc42 in control siRNA-treated (Ctrl, dark gray) and vimentin siRNA-treated (VIM siRNA, light gray) 3T3 cells, as well as mEF control (teal), mEF vimentin-null (VIM null, green) and mEF VIM siRNA (turquoise) and mEF vimentin-rescue (blue) cells plated on collagen. (B,C) Representative immunoblotting and quantification of (B) Rac1 activity in mEF WT (control, teal), VIM null (green) and VIM rescue (blue) cells and (C) Cdc42 activity in mEF WT and vimentin-null cells after paxillin siRNA (Pax siRNA) and paxillin–GFP plasmid transfection (Pax rescue). β-actin is shown as a loading control. Data in A–C were from three independent experiments and are reported as mean± s.e.m., **P*<0.05; ***P*<0.01; ****P*<0.001; *****P*<0.0001; ns, not significant (ordinary one-way ANOVA test used). (D) Evaluation of PAK autophosphorylation as an indicator of PAK activity in mEF control (teal) and mEF VIM null (green) cells plated on collagen for 3 h. Samples were immunoblotted for PAK phospho-S141 and -T423. Mean±s.e.m., *n*=3. **P*<0.05; ns, not significant (two-way ANOVA test used). (E) Quantification of PAK phosphorylation after Cdc42 inhibition by ML141 (10 μM) in WT (square, teal solid line), WT+ML141 (square, black dotted line), VIM null (circle, green solid line) and VIM null+ML141 (circle, gray dotted line) mEF cells plated on collagen for 3 h. Data were obtained from three independent experiments and reported as a mean ±s.e.m., **P*<0.05; ns, not significant (compared with control cells; ordinary one-way ANOVA test used). (F) Confocal images of 3T3 and mEF (control and VIM siRNA) cells plated on collagen-coated surfaces for 3 h to enable the initial formation of cell extensions. Cells were stained for actin (Rhodamine–phalloidin, white), myosin-10 (MyoX; anti-Myo10, cyan) and nuclei (DAPI, blue). Insets represent magnifications of areas marked by dashed boxes, showing cell protrusions stained with Myo10 as a filopodia marker. Scale bars: 20 μm. (G) 3T3 and mEF cells were transfected with scrambled siRNA (WT) or VIM siRNA, and imaged alongside VIM null mEF cells by light microscopy at 0, 4, 8 and 16 h to assess efficiency of cell migration. Dashed lines indicate the edge of the gap created in the culture cells. Scale bars: 100 μm. (H) Velocity of cell migration was calculated for each sample in G, followed by statistical analysis. The box plots indicate the 95% confidence interval, with the median indicated by a horizontal line, and the vertical bars illustrate the minimum and maximum value. *n*=3. *****P*<0.0001 (ordinary one-way ANOVA test used).

Journal of Cell Science (2021) 134, jcs254359. doi:10.1242/jcs.254359

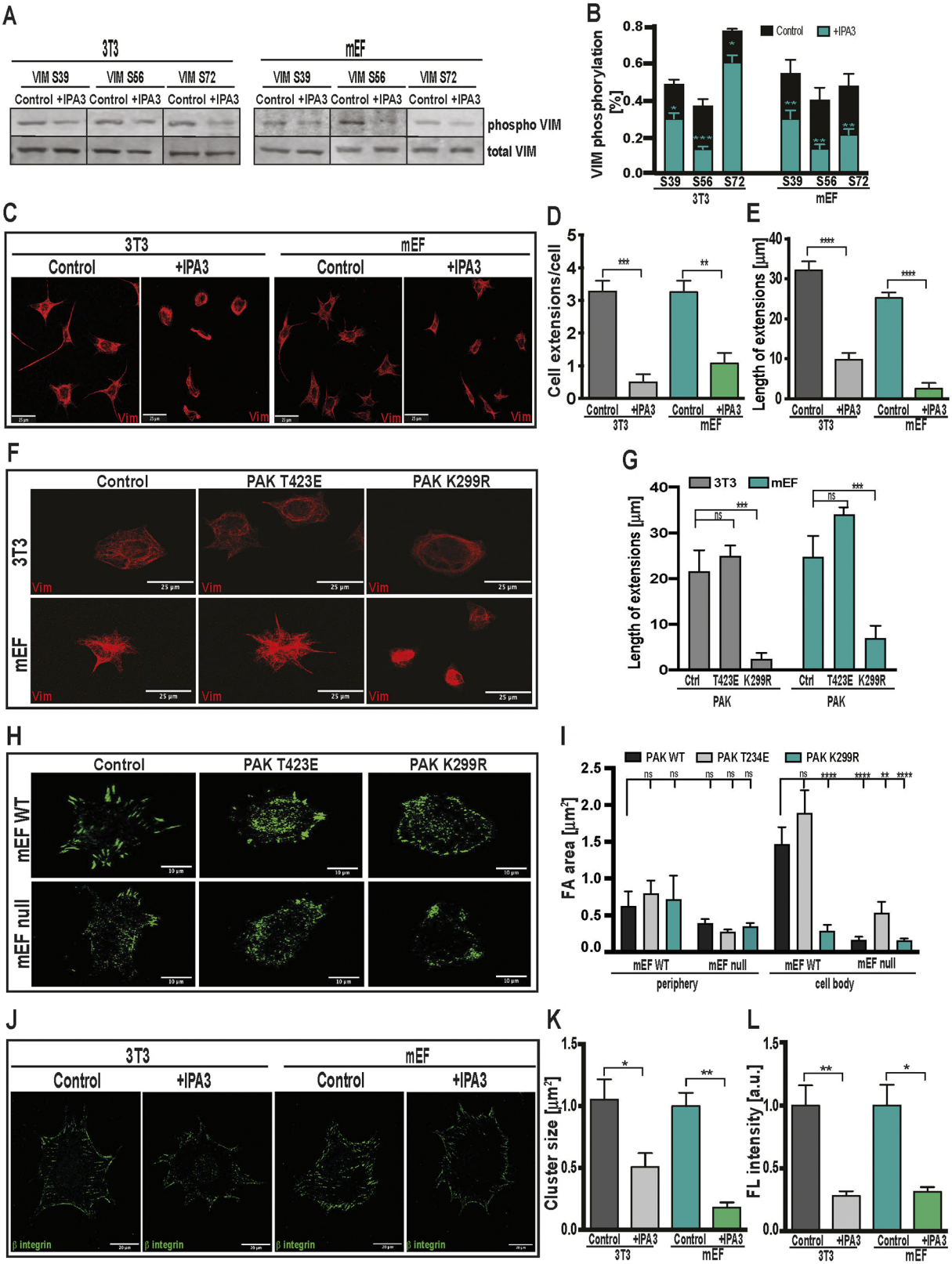

Fig. 6. See next page for legend.

cell extension length (Fig. 6G) in cells transfected with plasmids carrying PAK1 K299R or PAK1 T423E mutants (in addition to endogenous PAK1 expression; the controls in Fig. 6F–I show expression of WT PAK1 from a plasmid transfection). Cells treated with the plasmid carrying kinase-dead PAK1 K299R showed a greater than 70% reduction in cell extension length. In contrast, in cells transfected with the constitutively active PAK1 T423E, cell extension length was increased (by 15% for 3T3 cells and 37% for

Journal of Cell Science (2021) 134, jcs254359. doi:10.1242/jcs.254359

Fig. 6. PAK1 mediates vimentin phosphorylation and regulates cell extension formation. (A) Representative immunoblots of WT 3T3 and mEF cells treated for 3 h with vehicle (control) or with IPA3 (5 µM), a specific PAK inhibitor. Cells were cultured on collagen-coated dishes and immunoblotted with anti-vimentin (VIM) and anti-phospho S39, S56 and S72 vimentin antibodies. (B) Relative vimentin phosphorylation for control (black) and IPA3 treatment (teal) cells. All data are reported as mean±s.e.m., *n*=3, 50 cells per group. **P*<0.05; ***P*<0.01 (compared with control; two-way ANOVA test used). (C) Confocal images of 3T3 and mEF cells cultured on collagen and treated for 3 h with vehicle (control) or with IPA3. Cells were fixed and immunostained for vimentin (red). Scale bars: 25 µm. (D) Measurement of cell extensions per cell after treatment with IPA3, compared with control cells plated on collagen. 3T3 control cells (dark gray), 3T3+IPA3 (light gray), mEF control (teal), mEF+IPA3 (green). (E) Quantification of cell extension length after incubation with vehicle or IPA3 plated on collagen. 3T3 control cells (dark gray), 3T3+IPA3 (light gray), mEF control (teal), mEF+IPA3 (green). For D and E, cells were quantified using ImageJ (*n*=3, 20 cells per group), and data is shown as mean±s.e.m.. ***P*<0.01; ****P*<0.001; *****P*<0.0001 (two-way ANOVA test used). (F) Confocal images for 3T3 and mEF WT cells transfected with a plasmid carrying WT PAK1, or PAK1 mutant plasmids (T423E or K298R). Plasmid PAK1 T423E contained constitutively active PAK1, whereas plasmid PAK1 K298R contained kinase-dead PAK1. Cells were plated on a collagen-coated surface for 3 h, fixed and immunostained for vimentin. Scale bars: 25 µm. (G) Cell extension length based on confocal images. Quantification was performed using ImageJ. Data are reported as a mean± s.e.m. *n*=3, 20 cells per group. ****P*<0.001; ns, not significant (two-way ANOVA test used). (H) Representative confocal images for mEF WT and mEF vimentin-null cells treated with vehicle (control) or PAK1 mutant plasmids (T423E or K298R) and stained for paxillin. Scale bars: 10 µm. (I) Quantification of focal adhesion (FA) distribution with respect to the leading edge for mEF WT and vimentin-null cells treated with vehicle (control) or PAK1 mutant plasmids (T423E or K298R). Cell area was designated for cell periphery (1.75 µm from the leading edge) and cell body. PAK WT (black), PAK T234E (gray) and PAK K299R (teal). All data are reported as mean±s.e.m. *n*=3, 20 cells per group. ***P*<0.01; *****P*<0.0001; ns, not significant (two-way ANOVA test used). (J) Confocal images of 3T3 and mEF cells immunostained for β1 integrins (9EG7 clone, green), cultured on collagen and treated with vehicle (control) or IPA3. Scale bars: 20 µm. (K) Quantification of β1 integrin cluster size before and after treatments with IPA3 for 3T3 and mEF cells plated on collagen. 3T3 control cells (dark gray), 3T3+IPA3 (light gray), mEF control (teal), mEF+IPA3 (green). Data are mean±s.e.m. *n*=3, 25 cells per group. **P*<0.05; ***P*<0.01 (two-way ANOVA test used). (L) Flow cytometry-based estimation of the percentage of β1 integrin activation in response to the collagen-coated bead binding in the cell population treated with vehicle (control) or IPA3. 3T3 control cells (dark gray), 3T3+IPA3 (light gray), mEF control (teal), mEF+IPA3 (green). FL, fluorescence; a.u., arbitrary units. Flow cytometry data are reported as mean±s.e.m. *n*=3, 10,000 cells. **P*<0.05; ***P*<0.01 (two-way ANOVA test used).

mEFs). These results indicate that changes of cell morphology (in this instance, the formation of cell extensions) were related to inhibition of PAK1-dependent vimentin phosphorylation, which in turn reduced vimentin recruitment to focal adhesions. Further, we investigated whether treatment with IPA3 (Fig. S5A) and the various PAK mutants (Fig. 6H) affected the distribution of paxillin in focal adhesions. These data showed that alteration of vimentin assembly and loss of vimentin filaments was associated with paxillin recruitment into focal adhesions. We also examined the distribution of focal adhesions in the cell periphery and cell body. Transfection with a PAK dominant-negative mutant (K299R) reduced the sizes of focal adhesions for WT mEFs and vimentin-null mEFs by 5-fold and 9-fold, respectively. In cells transfected with the constitutively active PAK mutant (T234E), the size of focal adhesions was increased by 27% for WT mEFs and 5-fold for vimentin-null mEFs, compared with control cells (Fig. 6I). Furthermore, inhibition of PAK by IPA3 resulted in similar reductions of focal adhesion areas (Fig. S5B). These data were consistent with the distributions of the β1 integrin, suggesting that PAK1-dependent vimentin phosphorylation is involved in vimentin filament assembly and maturation. Further, we evaluated the impact of PAK-dependent vimentin phosphorylation on the activation of β1 integrin. In cells immunostained for active β1 integrin, confocal microscopy (Fig. 6J) showed that IPA3 inhibited the formation of β1 integrin clusters (Fig. 6K). These results were also consistent with flow cytometry assays showing that inhibition of vimentin phosphorylation blocked β1 integrin activation (Fig. 6L). Furthermore, we analyzed the effect of the PAK1 mutants on β1 integrin activity in vimentin-WT and -null mEFs. These data (Fig. S5C) indicate that inhibition of PAK1 kinase (K299R) caused a 38% and 15% reduction of β1 integrin activity in vimentin-WT and -null mEFs, respectively.

DISCUSSION

The ability of cells to spread, form extensions, migrate and remodel fibrillar collagen depends on their interactions with underlying matrix molecules (Discher et al., 2005). In addition to actin filaments and actin-binding proteins, vimentin filaments are thought to be centrally involved in cell migration during wound healing (Helfand et al., 2011; Mendez et al., 2010) and cancer invasion (Schoumacher et al., 2010). However, the mechanism of how vimentin regulates the formation of cell extensions in physiological remodeling of mature connective tissue is not well defined. Our central finding is that vimentin affects cell extension formation in a collagen-dependent manner and plays a key role in regulating β1 integrin activation and clustering through the control of talin and paxillin recruitment into focal adhesions. Notably, paxillin regulates Cdc42 activation (Hodge and Ridley, 2016; Iden and Collard, 2008; Jaffe and Hall, 2005), which in turn enables PAK1 activation, vimentin phosphorylation and induction of vimentin filament formation (Ding et al., 2020; Eriksson et al., 2004; Goto et al., 2002; Li et al., 2006). Taken together, these processes contribute to increased cell extension formation. Our data presented here indicate that vimentin in focal adhesions plays a central role as an adaptor protein, which may contribute to mesenchymal cell migration and extracellular matrix remodeling (Pinto et al., 2015; Terriac et al., 2017). These processes, which are associated with EMT, are important for tissue regeneration and repair in wound healing (Stone et al., 2016). Collectively, our results indicate that vimentin affects cell extension formation and cell adhesion by regulating β1 integrin activity and avidity in collagen-dependent manner (Fig. 7).

Vimentin filaments are involved in the determination of cell shape (Lowery et al., 2015; Mendez et al., 2010) and in the development and stabilization of cell extensions during cell migration on fibronectin (Ding et al., 2020). We found that in fibroblasts expressing vimentin, there was rapid formation and elongation of extensions in cells plated on fibronectin and collagen. While the vimentin-depleted cells showed reductions in the number and length of extensions, only the extension length was reduced in cells cultured on fibronectin. Consistent with these data, knockdown of vimentin also strongly affected cell area and circularity on collagen. Whereas cell area provides a general estimate of cell spreading, a reduction of circularity is consistent with the formation of membrane protrusions such as lamellipodia and filopodia (Uynuk-Ool et al., 2017) that are needed for cell migration through the collagen matrix.

Integrins are critically important adhesion receptors that regulate cell attachment to matrix proteins. For binding to collagen, cells use the β1 integrin (Maemura et al., 1995; Zeltz and Gullberg, 2016). The dynamic interaction between integrins and collagen is crucial for the stabilization of membrane protrusions and for the tension application to the ECM and retraction of the cell rear during cell migration; integrin recycling is central to the regulation of this

Journal of Cell Science (2021) 134, jcs254359. doi:10.1242/jcs.254359

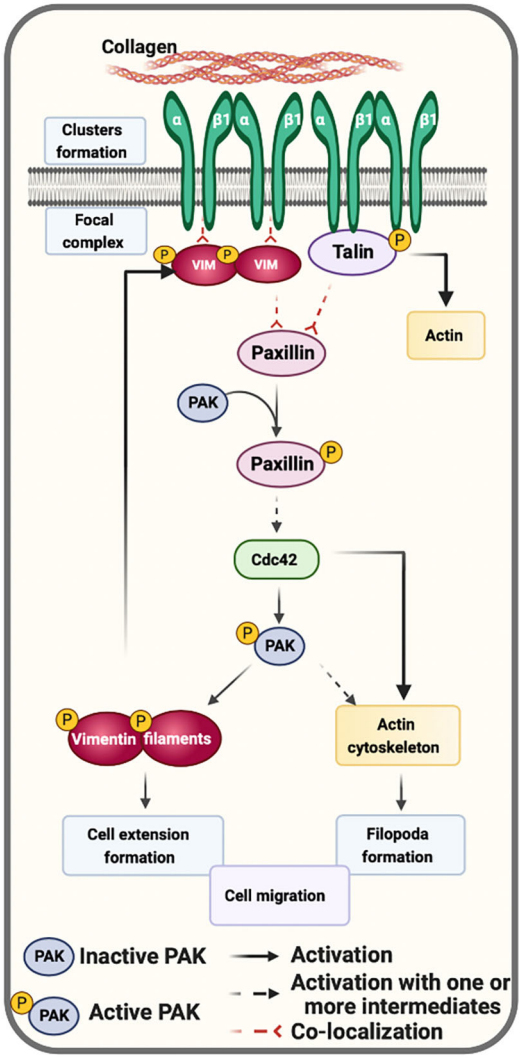

Fig. 7. Model of the role of vimentin in focal adhesion and cell extension formation in motile cells. Collagen-dependent integrin engagement recruits the structural proteins talin and vimentin (VIM). Vimentin colocalizes with β1 integrin and recruits paxillin to form new adhesions. After the initial formation of adhesions, additional focal adhesion proteins, such as talin, are recruited to form more stable and mature focal adhesions. Paxillin binds several proteins that contribute to Ccd42 activation. Further downstream, Cdc42 and PAK enhance vimentin phosphorylation. PAK is involved in activating Cdc42-stimulated reorganization of the actin cytoskeleton and vimentin filament assembly, which helps to promote cell motility. Diagram was created with BioRender.com.

process of adhesion turnover (Caswell et al., 2009). Expression of integrins can dynamically respond to changes in the cell environment, which enables cells to maintain their connection to the ECM (Desgrosellier and Cheresh, 2010; Hynes, 2009). When cells attach to collagen, the high abundance of this matrix protein ensures that it is always available for binding whenever an integrin briefly shifts to a high-affinity conformation (Arjonen et al., 2012). Our data show that vimentin depletion increases the total expression of β1 integrin and the membrane-associated fraction, which is activated in response to collagen binding. In light of these data, we investigated whether the increased β1 integrin affinity caused by vimentin deletion also affects cell adhesion. Flow cytometry and jet-wash evaluations of adhesion strength showed that cell–collagen adhesions were stronger after vimentin deletion, which is consistent with our finding of increased numbers of membrane-associated β1 integrin receptors and increased activation. These data are consistent with previous studies linking integrin activation to reduced receptor recycling rates and increased lysosomal degradation (De Franceschi et al., 2015). Analysis of β1 integrin activation in cells plated on fibrinogen or fibronectin-coated surfaces showed no prominent differences after vimentin deletion.

The ability of cells to sense and respond to collagen depends on spatially and temporally specific alterations of integrin conformation, which in turn regulates activation and aggregation processes (Baade et al., 2019; Liu et al., 2015b; Puklin-Faucher and Sheetz, 2009) that are linked to cluster formation (Welf et al., 2012). Our data show that vimentin also critically regulates β1 integrin receptor clustering on collagen. Despite enhanced integrin affinity and activation after vimentin depletion, integrin clusters remained much smaller than in WT cells. Moreover, we found an inverse relation between the size of β1 integrin clusters and the number of clusters, which is consistent with earlier studies showing that vimentin localizes to nascent adhesions (Terriac et al., 2017) and promotes integrin clustering. These results suggest that vimentin plays a critical role in linking β1 integrin activation to cluster formation in collagen-dependent manner, which is also supported by the vimentin rescue experiments. Previous data has shown that the focal contacts of cultured fibroblasts derived from vimentin-null mice are less regular, less distinct and less mechanically stable than those of WT control cells (Battaglia et al., 2018).

When integrins are activated and bound to matrix ligands, they promote the aggregation of hundreds of adaptors and signaling molecules at their cytoplasmic tails to enable the assembly of a dynamic, macromolecular adhesion complex (Winograd-Katz et al., 2014). The clustering of β1 integrin tail domains leads to the recruitment of talin and paxillin, which in turn creates a platform for proteins that are indirectly linked to integrins, such as PAK and α-actinin (Puklin-Faucher and Sheetz, 2009; Liu et al., 2015a,b; Baade et al., 2019). With mass spectrometry analysis and confirmations by immunoblotting, we assessed the impact of vimentin deletion on proteins in adhesion complexes bound to collagen. Collectively these data indicate that the observed increase of β1 integrin activation in vimentin-null cells is related to higher abundance of talin cell adhesions and talin-dependent, ‘inside-out’ integrin signaling. Previous data has shown that vimentin localizes to cell adhesions at discrete stages of maturation (Terriac et al., 2017). Our findings showed that only filamentous vimentin colocalized with talin, whereas small vimentin particles were in close proximity with talin.

As paxillin colocalizes with talin near the plasma membrane (Dong et al., 2016; Kanchanawong et al., 2010), talin may also interact with vimentin. Indeed, our immunoprecipitation experiments showed association of vimentin and talin in cells migrating on fibrillar collagen. We found that loss of vimentin was associated with decreased recruitment of paxillin into adhesion complexes and that vimentin expression levels were associated with the number and size of adhesion plaques. The colocalization of talin with vimentin filaments suggests that vimentin was incorporated into cell adhesions and may affect its interactions with paxillin. In support of this notion is the previous observation that vimentin expression in epithelial cells increases paxillin turnover in focal adhesions by 4-fold (Mendez et al., 2010). Previous data also indicate that vimentin interactions with focal adhesion proteins regulate the formation of the adhesions (Dave et al., 2013; Menko et al., 2014; Terriac et al., 2017; Tsuruta and Jones, 2003). Taken together, these data indicate that the association of vimentin with

paxillin and talin enables the maturation of integrin clusters and the maintenance of collagen adhesion structures that are involved in 'inside-out' integrin signaling.

Paxillin is recruited into adhesion structures and, when phosphorylated, paxillin induces Cdc42 activation (Hodge and Ridley, 2016; Iden and Collard, 2008), which in turn drives filopodia formation and cell migration (Chen et al., 2000; Kozma et al., 1995; Nobes and Hall, 1999). We found that vimentin contributes to the activation of Cdc42 and Rac1, and in turn, the formation of cell protrusions. Depletion of vimentin was strongly associated with diminished Cdc42 and Rac1 activity, which correlates with the reduced cell extension formation and cell migration we observed. Notably, Cdc42 is downstream of PAK and enables PAK activation (Rane and Minden, 2014). Our data support the idea that vimentin plays an important role in cell extension formation through control of Cdc42-dependent PAK activation. Moreover, by enhancing recruitment of paxillin into focal adhesions, vimentin may contribute to Cdc42 activation through a paxillin-dependent pathway. Recent data indicate that the paxillin-related focal adhesion protein Hic-5 (also known as TGBB1I1), stabilizes the vimentin network by modulation of Rho GTPases, and its ablation leads to the disassembly of vimentin filaments (Vohnoutka et al., 2019), findings which underpin the involvement of vimentin in adhesion biology.

The formation of cell extensions strongly depends on PAK1-dependent vimentin phosphorylation and filament assembly (Ding et al., 2020). Our findings are consistent with previous data demonstrating that PAK inhibition abrogates vimentin S39, S56 and S72 phosphorylation, as well as vimentin spatial reorganization and cell extension formation (Ding et al., 2020). Furthermore, we found that alterations of vimentin structure are associated with the reduction of β1 integrin cluster size, which is consistent with earlier data linking small vimentin particles with nascent cell adhesions (Terriac et al., 2017).

The formation of integrin clusters is thought to depend on interacting processes that regulate the production, concentration and diffusion of integrin-activating proteins (Welf et al., 2012). Our findings indicate that vimentin affects the organization, structure and function of cell–collagen adhesions by suppressing β1 integrin activation, thereby resulting in well-organized, mature integrin clusters. In contrast, loss of vimentin dissipates local concentrations of integrins, which curtails the growth of integrin clusters and collagen adhesions. Notably, fine tuning of cell adhesion is essential for the formation of cell extensions. In this context, we propose that vimentin filaments are essential for the recruitment of paxillin into adhesion complexes and in the regulation of Cdc42 and PAK1 activation, which are also required for the formation of cell extensions. These processes are ultimately dependent on vimentin phosphorylation mediated by PAK1, which promotes vimentin filament maturation of cell extensions and migration on collagen.

MATERIALS AND METHODS

Reagents and antibodies

Rat anti-β1 integrin (clone KMI6, ab95623), anti-phospho-vimentin (S72, EP1070Y), goat anti-rabbit IgG H&L (DyLight 488 conjugated, ab150077), rabbit anti-Cdc42 (ab155940), rat anti-α-actinin (EA-53, ab9465), rabbit anti-paxillin (Y113, ab32084), mouse anti-talin1 (ab157808) and anti-PAK1 (phospho S144, ab40795) antibodies were purchased from Abcam (Cambridge, MA). Rabbit anti-phospho-vimentin (S56, 3877S), anti-phospho-vimentin (S39, 13614S), rabbit anti-PAK1 (2602S), rabbit anti-phospho-PAK1 T423 (2601) and rabbit anti-Rac1 (2465S) antibodies were obtained from Cell Signaling Technology (Danvers, MA). Chicken anti-vimentin antibody (N13300-223) was purchased from Novus Biologicals (Littleton, CO). Goat anti-DDR2 antibody (AF2538) was from R&D Systems (Minneapolis, MN). Fibronectin, fibrinogen, ML141 (Cdc42/Rac1 inhibitor), IPA-3 (PAK1 inhibitor), mouse anti-β-actin (A1978), rabbit anti-myosin-10 (APA024223), DAPI was obtained from Sigma-Aldrich (St. Louis, MO). Fluorescent 2 µm beads (09847-5) were from BioTrend (Germany). Alexa Fluor 488-conjugated goat anti-mouse antibody (A11001) Alexa Fluor 568-conjugated goat anti-rabbit antibody (A-11011) and Rhodamine–phalloidin, were from Invitrogen (Carlsbad, CA). Alexa Fluor 647-conjugated AffiniPure F (ab')$_2$ fragment donkey anti-chicken IgY (H+L) (703-605-155) was from Jackson ImmunoResearch (West Grove, PA). Rat anti-CD29 (β1 integrin subunit, 9EG7 clone, 553715) was from BD Biosciences (Mississauga, ON). ON-TARGETplus non-target pool (5 nmol), ON-TARGETplus siRNA reagents VIM (5 nmol), ON-TARGETplus siRNA Reagents Pax (5 nmol) and ON-TARGETplus siRNA Tln1 siRNA 3′ UTR CGC and 3′ UTR CAG (custom siRNA, sequences used are available upon request; standard 0.015 µmol regular) were obtained from Horizon (Lafayette, CO). DharmaFECT1 transfection reagent was purchased from Dharmacon (Lafayette, CO). FuGENE HD transfection reagent, BCA protein assay (Pierce), RIPA lysis buffer, IP lysis buffer and Lipofectamine 3000 reagent were obtained from Thermo Fisher Scientific (Mississauga, ON). Type I bovine collagen solution (3 mg/ml) was from Advanced BioMatrix (San Diego, CA). Plasmids containing full-length PAK1 cloned into pCMV6 (plasmid 12209), catalytically inactive mutant PAK1 (K299R; plasmid 12210) or constitutively active PAK1 (T423E; plasmid 12208), GFP–Paxillin (plasmid 15233), GFP–talin1 (plasmid 26724) were obtained from Addgene (Cambridge, MA). pCMV3-mVIM–GFP-spark plasmid was from Sino Biological Inc (Chesterbrook, PA). The FITC anti-rat IgG2a antibody clone MRG2a-83 (407506) was obtained from BioLegend (San Diego, CA)

Cells and transfection

Mouse NIH-3T3 fibroblasts were obtained from David Calderwood (Yale University, New Haven, CT). Wild-type (mEF WT) and vimentin-null (mEF null) mouse immortalized embryonic fibroblasts, derived from WT and vimentin-knockout mice, respectively, were passaged from a cell line originally isolated by the laboratory of J. Ericsson (Abo Akademi University, Turku, Finland). Vimentin-rescue mEF cells were prepared by transfection of mEF null cells with pCMV3-mVIM–GFP-spark plasmid. Cells were cultured at 37°C in complete DMEM containing 10% Hyclone fetal bovine serum (3T3 cells) or FBS (mEFs) and 10% (v/v) antibiotics. For vimentin siRNA transfection, cells were trypsinized and plated on 100 mm dishes to 60–70% confluence. Cells were treated with Dharmacon ON-TARGET siRNAs plus transfection reagents or with non-targeting control siRNA, following the manufacturer's protocol. To obtain talin1 or paxillin KD cells, mEFs were transfected with respective siRNAs using Lipofectamine 3000. Talin1 or paxillin re-expression was done by co-transfection with GFP–talin1- and GFP–paxillin-containing plasmids, respectively. Cells were grown for 48 h, lysed in RIPA buffer, and whole-cell lysates were collected. Protein concentrations were determined using a BCA protein assay (Pierce). Equal amounts of proteins from each treatment condition were separated on 8% and 10% acrylamide gels and immunoblotted to estimate the efficiency of the KD. For PAK1 mutant experiments, cells were transfected using FuGENE HD DNA transfection reagent according to the manufacturer's instructions.

Immunoblotting

Cells were plated on collagen-coated 100 mm dishes and lysed with RIPA buffer (25 mM Tris-HCl pH 7.6, 150 mM NaCl, 1% NP-40, 1% sodium deoxycholate and 0.1% SDS) supplemented with 1 mM PMSF, 1 mM $NaVO_3$ and 10 µg/ml protease inhibitor cocktail. Equal amounts of proteins were loaded on 8% or 10% polyacrylamide gels, resolved by SDS–PAGE and transferred to nitrocellulose membranes for 18 h. The membranes were blocked with TBS containing 5% BSA for 1 h followed by overnight incubation with primary antibodies (anti-β-actin was used at a dilution of 1:3000, other primary antibodies were used at a dilution of 1:5000). Membranes were washed and incubated with respective secondary antibodies (1:5000) for 1 h in TBS supplemented with 0.1% Tween-20 at

Journal of Cell Science (2021) 134, jcs254359. doi:10.1242/jcs.254359

room temperature. All immunoblots were performed in triplicate. Blots were visualized with a Li-Cor Odyssey imager (Lincoln, NB) and quantified densitometrically using ImageJ software (NIH, Bethesda, MD).

Immunostaining and microscopy analysis

In most experiments, cells were cultured on monomeric collagen (0.1 mg/ml), fixed with 1% paraformaldehyde for 15 min, permeabilized in 0.2% Triton X-100 for 10 min, and blocked with 1% BSA. Samples were incubated with appropriate primary antibodies for 1 h at 37°C. Cells were washed with PBS following secondary antibody incubation. In most experiments, cells were stained with DAPI in NP-40 (10 µg/ml) and with Rhodamine–phalloidin for actin filaments. For studies of vimentin, phospho-vimentin (S39, S56 and S72), β1 integrin, paxillin and myosin-10, samples were incubated with appropriate primary antibodies (1:100 in PBS containing 0.2% BSA) for 1 h at 37°C. Cells were washed with PBS and stained with secondary antibody (1:200). Images were obtained with a TCS SP8 confocal microscope (Leica Microsystems, Wetzlar, Germany) equipped with a ×40 oil-immersion objective lens, a Zeiss LSM 800 confocal microscope (Zeiss, Germany) equipped with a ×63 oil-immersion objective lens, and an Olympus SpinSR10 spinning-disk confocal super-resolution microscope. Analysis and quantification of acquired images were done with ImageJ software. The mean cell surface area was determined using the cell outliner plugin (https://imagej.nih.gov/ij/plugins/cell-outliner.html).

Cell extensions were defined as cell protrusions that were >10 µm as measured from the cell centroid to the tip of each extension. Pearson correlation coefficients were determined with JACoP (Just Another Colocalization Plugin; https://imagej.nih.gov/ij/plugins/track/jacop.html) in Fiji (https://imagej.net/Fiji). The spatial distribution of β1integrin clusters with respect to the leading edge was determined using a macro that indicated two separate masks for the cell periphery (1.75 µm from the leading edge) and for the cell body excluding the area of cell periphery. The number and area of β1 integrin clusters were quantified on fluorescence images acquired on the confocal microscope according to the method described by Coelho et al. (2017). Briefly, in Fiji the image background was subtracted using the sliding paraboloid; the local image contrast was enhanced with the CLACHE plugin; the background was minimized with mathematical exponential (EXP); and the brightness and contrast were adjusted automatically followed by auto thresholding. The number and area of β1 integrin clusters were obtained with the Analyze Particles program in Fiji.

Flow cytometry

For quantification of the total abundance of β1 integrin and the activated fraction of β1 integrin, cells were plated on fibronectin (10 µg/ml)-coated or collagen (1 mg/ml)-coated 100 mm dishes for 3 h (Segal et al., 2001). Cells were washed with ice-cold PBS, scraped immediately with Versene solution and fixed with 1% paraformaldehyde. Cells were washed and incubated with primary antibodies (KMI6 for total β1 integrin and 9EG7 for activated β1 integrin) for 1 h at 37°C. Cells were washed with PBS, stained with FITC-conjugated anti-rat secondary antibodies and analyzed by flow cytometry (Sony SA3800 Spectral Analyzer).

Fluorescent bead assays

Collagen-coated latex beads (2 µm) were prepared as previously described (Lee et al., 1996). Yellow-green fluorescent beads were incubated with 1 mg/ml acidic solution of bovine type I collagen and neutralized with 1 M NaOH to pH 7.4 to facilitate fibril formation on the bead's surface. Beads were incubated with agitation at 37°C for 1 h. Beads were pelleted, resuspended in PBS, briefly sonicated and counted using a hemocytometer. Cells were counted electronically, and collagen-coated beads were loaded on to the top surfaces of cells at an 8:1 bead:cell ratio for 3 h. To reduce the inclusion of cells bearing loosely or non-specifically bound beads, cells were washed (in PBS), trypsinized and resuspended in DMEM (Segal et al., 2001). BSA (0.01 mg/ml)-, fibrinogen (1 mg/ml)- and poly-L-lysine (0.1%)- coated yellow-green beads (2 µm) were prepared as described above. Samples were analyzed by flow cytometry (Sony SA3800 Spectral Analyzer) to estimate the percentage of cells with bound collagen-coated fluorescent beads.

Bead binding strength

The relative binding strength of cells to fibrillar collagen or fibrinogen-coated beads was estimated by a shear wash assay (Chong et al., 2007). Experiments were performed as described previously (Coelho et al., 2017) using cells plated on 24-well tissue culture plates at 80–90% confluency. FITC-labeled beads (2 µm) were coated with 1 mg/ml collagen solution as described above. The collagen-coated beads were added to the serum-free medium on the top of cells (8:1 bead:cell ratio) for 2 h. The cells were then subjected to increasing numbers of washes (1–16 washes, shear stress of 3.5 Pa). Cells were fixed with 4% paraformaldehyde for 10 min and stained with DAPI (5 µg/ml). Bound beads and nuclei were visualized by fluorescence microscopy and counted by using the Cell counter plugin in ImageJ (https://imagej.nih.gov/ij/plugins/cell-counter.html).

Immunoprecipitation

Cells were lysed in IP lysis buffer (25 mM Tris-HCl pH 7.4, 150 mM NaCl, 1 mM EDTA, 1% NP-40 and 5% glycerol) containing 1 mM PMSF, 1 mM NaVO3, 10 µg/ml leupeptin, and 10 µg/ml aprotinin. Equal amounts of protein from cleared extracts were immunoprecipitated with the Dyna-beads Protein G (Life Technologies) according to the manufacturer's protocol (Invitrogen, Carlsbad, CA, USA) with primary antibodies overnight. Beads were separated using a magnetic stand and washed with an IP lysis buffer. Immunoprecipitated proteins were separated from beads by resuspending in Laemmli sample buffer and boiling for 10 min. The beads were sedimented, and lysates were analyzed by western blotting.

PBD pulldown assay

The Cdc42 and Rac1 activation assay was performed with PAK1 binding domain (PBD) bound to glutathione–Sepharose beads. Fibroblasts were plated on collagen-coated 100 mm dishes and incubated for 3 h. Adherent cells were lysed with RIPA buffer. Lysates were clarified by centrifugation, equalized for total volume and protein concentration, and rotated overnight with 30 g of purified PBD-bound beads. The beads were pelleted and washed in PBS, resuspended in Laemmli buffer and boiled. Equal amounts of protein were separated by SDS–PAGE using 15% gels. The Cdc42 activation assay was performed with antibodies against Cdc42, and Rac activation was assayed with antibodies against Rac1.

Isolation of focal adhesion proteins

Cells were cultured to 80–90% confluence on 100 mm tissue culture dishes and then incubated with 1 mg/ml collagen-coated magnetite beads (Sigma-Aldrich). Focal adhesion complexes were isolated from cells as described previously (Wang et al., 2009). In brief, cells were washed with ice-cold PBS to remove unbound beads and scraped into ice-cold cytoskeleton extraction buffer (CKSB; 0.5% Triton X-100, 50 mM NaCl, 300 mM sucrose, 3 mM $MgCl_2$, 20 µg/ml aprotinin, 1 µg/ml leupeptin, 1 µg/ml pepstatin, 1 mM phenylmethylsulfonyl fluoride and 10 mM PIPES, pH 6.8). The cell–bead suspension was briefly sonicated, and the beads were isolated from the lysate using a magnetic separation stand. The beads were resuspended in fresh ice-cold CKSB and re-isolated magnetically. Then, beads were washed in CSKB, sedimented by centrifugation, resuspended in Laemmli sample buffer and boiled for 10 min to allow the collagen-associated complexes to dissociate from the beads. The beads were separated magnetically, and lysates were analyzed by western blotting.

Mass spectrometry

Vimentin-WT and -null cells were incubated with collagen-coated magnetite beads as described above. Proteins were eluted from beads with 10 mM DTT at 60°C for 1 h. Alkylation was performed using 20 mM iodoacetamide at room temperature for 45 min in the dark. Trypsin (2 µg; Pierce) was added to the samples, which were rotated overnight at 37°C. The eluted proteins were lyophilized in a Speedvac and desalted using a Millipore C18 ziptip. Subsequently, 0.1% formic acid was added to the sample, which was then air-dried with an evaporator. Lyophilized samples were analyzed using a Thermo Scientific Orbitrap Q exactive HFX at the Hospital for Sick Children SPARC BioCentre (Toronto, ON, Canada). Scaffold 4.10 (Proteome Software, Portland, OR, USA) was used for analyzing search results, calculating *P*-values for each peptide match and matching peptide spectra.

Statistical analysis

Statistical significance ($P<0.05$) was determined using the unpaired *t*-test for two samples or ANOVA for multiple samples. For analysis of the spatial relationship of proteins in cultured cells, Pearson correlation was used (Bolte and Cordelieres, 2006). Analyses were performed with GraphPad Prism 8 software. All experiments were performed at least three independent times in triplicates on separate days. Bar charts show mean±s.e.m.

Acknowledgements

The authors thank Joao Bronze de Firmino from the imaging facility in the Faculty of Dentistry, University of Toronto for help with developing the Fiji macro and the quantification of β1 integrin distribution. The authors thank the SPARC BioCentre - Molecular Analysis, The Hospital for Sick Children, Toronto, Canada, for assistance with mass spectrometry.

Competing interests

The authors declare no competing or financial interests.

Author contributions

Conceptualization: Z.O.-P, P.A.J., C.A.M.; Methodology: Z.O.-P., W.L., C.A.M.; Validation: Z.O.-P., I.D., J.T., S.A., P.D.A., R.S.L., A.E.P., C.A.M.; Formal analysis: Z.O.-P., W.L.; Investigation: Z.O.-P., P.A.J., C.A.M.; Data curation: Z.O.-P., I.D., W.L., J.T., S.A., P.D.A., R.S.L., A.E.P.; Writing - original draft: Z.O.-P., C.A.M.; Writing - review & editing: Z.O.-P., P.A.J., C.A.M.; Visualization: Z.O.-P., C.A.M.; Supervision: C.A.M.; Project administration: C.A.M.; Funding acquisition: C.A.M.

Funding

This study was supported by a Canadian Institutes of Health Research (CIHR) grant (MOP-416228) and by Canada Research Chairs (C.A.M.).

Data availability

The mass spectrometry datasets are available upon request from the first author.

Supplementary information

Supplementary information available online at
https://jcs.biologists.org/lookup/doi/10.1242/jcs.254359.supplemental

Peer review history

The peer review history is available online at
https://jcs.biologists.org/lookup/doi/10.1242/jcs.254359.reviewer-comments.pdf

References

Acloque, H., Adams, M. S., Fishwick, K., Bronner-Fraser, M. and Nieto, M. A. (2009). Epithelial-mesenchymal transitions: the importance of changing cell state in development and disease. *J. Clin. Invest.* **119**, 1438-1449. doi:10.1172/JCI38019

Anthis, N. J., Wegener, K. L., Ye, F., Kim, C., Goult, B. T., Lowe, E. D., Vakonakis, I., Bate, N., Critchley, D. R., Ginsberg, M. H. et al. (2009). The structure of an integrin/talin complex reveals the basis of inside-out signal transduction. *EMBO J.* **28**, 3623-3632. doi:10.1038/emboj.2009.287

Arjonen, A., Alanko, J., Veltel, S. and Ivaska, J. (2012). Distinct recycling of active and inactive beta1 integrins. *Traffic* **13**, 610-625. doi:10.1111/j.1600-0854.2012.01327.x

Baade, T., Paone, C., Baldrich, A. and Hauck, C. R. (2019). Clustering of integrin beta cytoplasmic domains triggers nascent adhesion formation and reveals a protozoan origin of the integrin-talin interaction. *Sci. Rep.* **9**, 5728. doi:10.1038/s41598-019-42002-6

Battaglia, R. A., Delic, S., Herrmann, H. and Snider, N. T. (2018). Vimentin on the move: new developments in cell migration. *F1000Res* **7**, 1796. doi:10.12688/f1000research.15967.1

Bolte, S. and Cordelieres, F. P. (2006). A guided tour into subcellular colocalization analysis in light microscopy. *J. Microsc.* **224**, 213-232. doi:10.1111/j.1365-2818.2006.01706.x

Burgstaller, G., Gregor, M., Winter, L. and Wiche, G. (2010). Keeping the vimentin network under control: cell-matrix adhesion-associated plectin 1f affects cell shape and polarity of fibroblasts. *Mol. Biol. Cell* **21**, 3362-3375. doi:10.1091/mbc.e10-02-0094

Calderwood, D. A., Campbell, I. D. and Critchley, D. R. (2013). Talins and kindlins: partners in integrin-mediated adhesion. *Nat. Rev. Mol. Cell Biol.* **14**, 503-517. doi:10.1038/nrm3624

Case, L. B. and Waterman, C. M. (2015). Integration of actin dynamics and cell adhesion by a three-dimensional, mechanosensitive molecular clutch. *Nat. Cell Biol.* **17**, 955-963. doi:10.1038/ncb3191

Caswell, P. T., Vadrevu, S. and Norman, J. C. (2009). Integrins: masters and slaves of endocytic transport. *Nat. Rev. Mol. Cell Biol.* **10**, 843-853. doi:10.1038/nrm2799

Chen, F., Ma, L., Parrini, M. C., Mao, X., Lopez, M., Wu, C., Marks, P. W., Davidson, L., Kwiatkowski, D. J., Kirchhausen, T. et al. (2000). Cdc42 is required for PIP(2)-induced actin polymerization and early development but not for cell viability. *Curr. Biol.* **10**, 758-765. doi:10.1016/S0960-9822(00)00571-6

Chong, S. A., Lee, W., Arora, P. D., Laschinger, C., Young, E. W., Simmons, C. A., Manolson, M., Sodek, J. and McCulloch, C. A. (2007). Methylglyoxal inhibits the binding step of collagen phagocytosis. *J. Biol. Chem.* **282**, 8510-8520. doi:10.1074/jbc.M609859200

Coelho, N. M., Arora, P. D., van Putten, S., Boo, S., Petrovic, P., Lin, A. X., Hinz, B. and McCulloch, C. A. (2017). Discoidin domain receptor 1 mediates myosin-dependent collagen contraction. *Cell Rep* **18**, 1774-1790. doi:10.1016/j.celrep.2017.01.061

Cox, T. R. and Erler, J. T. (2011). Remodeling and homeostasis of the extracellular matrix: implications for fibrotic diseases and cancer. *Dis. Model. Mech.* **4**, 165-178. doi:10.1242/dmm.004077

Critchley, D. R. (2009). Biochemical and structural properties of the integrin-associated cytoskeletal protein talin. *Annu. Rev. Biophys.* **38**, 235-254. doi:10.1146/annurev.biophys.050708.133744

Dave, J. M., Kang, H., Abbey, C. A., Maxwell, S. A. and Bayless, K. J. (2013). Proteomic profiling of endothelial invasion revealed receptor for activated C kinase 1 (RACK1) complexed with vimentin to regulate focal adhesion kinase (FAK). *J. Biol. Chem.* **288**, 30720-30733. doi:10.1074/jbc.M113.512467

De Franceschi, N., Hamidi, H., Alanko, J., Sahgal, P. and Ivaska, J. (2015). Integrin traffic - the update. *J. Cell Sci.* **128**, 839-852. doi:10.1242/jcs.161653

Deacon, S. W., Beeser, A., Fukui, J. A., Rennefahrt, U. E., Myers, C., Chernoff, J. and Peterson, J. R. (2008). An isoform-selective, small-molecule inhibitor targets the autoregulatory mechanism of p21-activated kinase. *Chem. Biol.* **15**, 322-331. doi:10.1016/j.chembiol.2008.03.005

Delorme-Walker, V. D., Peterson, J. R., Chernoff, J., Waterman, C. M., Danuser, G., DerMardirossian, C. and Bokoch, G. M. (2011). Pak1 regulates focal adhesion strength, myosin IIA distribution, and actin dynamics to optimize cell migration. *J. Cell Biol.* **193**, 1289-1303. doi:10.1083/jcb.201010059

Desgrosellier, J. S. and Cheresh, D. A. (2010). Integrins in cancer: biological implications and therapeutic opportunities. *Nat. Rev. Cancer* **10**, 9-22. doi:10.1038/nrc2748

Ding, I., Ostrowska-Podhorodecka, Z., Lee, W., Liu, R. S. C., Carneiro, K., Janmey, P. A. and McCulloch, C. A. (2020). Cooperative roles of PAK1 and filamin A in regulation of vimentin assembly and cell extension formation. *Biochim. Biophys. Acta. Mol. Cell Res.* **1867**, 118739. doi:10.1016/j.bbamcr.2020.118739

Discher, D. E., Janmey, P. and Wang, Y. L. (2005). Tissue cells feel and respond to the stiffness of their substrate. *Science* **310**, 1139-1143. doi:10.1126/science.1116995

Dong, J. M., Tay, F. P., Swa, H. L., Gunaratne, J., Leung, T., Burke, B. and Manser, E. (2016). Proximity biotinylation provides insight into the molecular composition of focal adhesions at the nanometer scale. *Sci. Signal.* **9**, rs4. doi:10.1126/scisignal.aaf3572

Eriksson, J. E., He, T., Trejo-Skalli, A. V., Harmala-Brasken, A. S., Hellman, J., Chou, Y. H. and Goldman, R. D. (2004). Specific in vivo phosphorylation sites determine the assembly dynamics of vimentin intermediate filaments. *J. Cell Sci.* **117**, 919-932. doi:10.1242/jcs.00906

Feng, Z., Wagatsuma, Y., Kikuchi, M., Kosawada, T., Nakamura, T., Sato, D., Shirasawa, N., Kitajima, T. and Umezu, M. (2014). The mechanisms of fibroblast-mediated compaction of collagen gels and the mechanical niche around individual fibroblasts. *Biomaterials* **35**, 8078-8091. doi:10.1016/j.biomaterials.2014.05.072

Geiger, B., Bershadsky, A., Pankov, R. and Yamada, K. M. (2001). Transmembrane crosstalk between the extracellular matrix–cytoskeleton crosstalk. *Nat. Rev. Mol. Cell Biol.* **2**, 793-805. doi:10.1038/35099066

Goto, H., Tanabe, K., Manser, E., Lim, L., Yasui, Y. and Inagaki, M. (2002). Phosphorylation and reorganization of vimentin by p21-activated kinase (PAK). *Genes Cells* **7**, 91-97. doi:10.1046/j.1356-9597.2001.00504.x

Grinnell, F., Rocha, L. B., Iucu, C., Rhee, S. and Jiang, H. (2006). Nested collagen matrices: a new model to study migration of human fibroblast populations in three dimensions. *Exp. Cell Res.* **312**, 86-94. doi:10.1016/j.yexcr.2005.10.001

Hall, A. (2005). Rho GTPases and the control of cell behaviour. *Biochem. Soc. Trans.* **33**, 891-895. doi:10.1042/BST0330891

Hantgan, R. R., Stahle, M. C. and Lord, S. T. (2010). Dynamic regulation of fibrinogen: integrin alphaIIbbeta3 binding. *Biochemistry* **49**, 9217-9225. doi:10.1021/bi1009858

Helfand, B. T., Mendez, M. G., Murthy, S. N., Shumaker, D. K., Grin, B., Mahammad, S., Aebi, U., Wedig, T., Wu, Y. I., Hahn, K. M. et al. (2011). Vimentin organization modulates the formation of lamellipodia. *Mol. Biol. Cell* **22**, 1274-1289. doi:10.1091/mbc.e10-08-0699

Hodge, R. G. and Ridley, A. J. (2016). Regulating Rho GTPases and their regulators. *Nat. Rev. Mol. Cell Biol.* **17**, 496-510. doi:10.1038/nrm.2016.67

Hynes, R. O. (2009). The extracellular matrix: not just pretty fibrils. *Science* **326**, 1216-1219. doi:10.1126/science.1176009

Iden, S. and Collard, J. G. (2008). Crosstalk between small GTPases and polarity proteins in cell polarization. *Nat. Rev. Mol. Cell Biol.* **9**, 846-859. doi:10.1038/nrm2521

Jaffe, A. B. and Hall, A. (2005). Rho GTPases: biochemistry and biology. *Annu. Rev. Cell Dev. Biol.* **21**, 247-269. doi:10.1146/annurev.cellbio.21.020604.150721
Kaimori, A., Potter, J., Kaimori, J. Y., Wang, C., Mezey, E. and Koteish, A. (2007). Transforming growth factor-beta1 induces an epithelial-to-mesenchymal transition state in mouse hepatocytes in vitro. *J. Biol. Chem.* **282**, 22089-22101. doi:10.1074/jbc.M700998200
Kanchanawong, P., Shtengel, G., Pasapera, A. M., Ramko, E. B., Davidson, M. W., Hess, H. F. and Waterman, C. M. (2010). Nanoscale architecture of integrin-based cell adhesions. *Nature* **468**, 580-584. doi:10.1038/nature09621
Kim, C., Ye, F. and Ginsberg, M. H. (2011). Regulation of integrin activation. *Annu. Rev. Cell Dev. Biol.* **27**, 321-345. doi:10.1146/annurev-cellbio-100109-104104
Kim, H., Nakamura, F., Lee, W., Hong, C., Perez-Sala, D. and McCulloch, C. A. (2010). Regulation of cell adhesion to collagen via beta1 integrins is dependent on interactions of filamin A with vimentin and protein kinase C epsilon. *Exp. Cell Res.* **316**, 1829-1844. doi:10.1016/j.yexcr.2010.02.007
Klapholz, B. and Brown, N. H. (2017). Talin - the master of integrin adhesions. *J. Cell Sci.* **130**, 2435-2446. doi:10.1242/jcs.190991
Kozma, R., Ahmed, S., Best, A. and Lim, L. (1995). The Ras-related protein Cdc42Hs and bradykinin promote formation of peripheral actin microspikes and filopodia in Swiss 3T3 fibroblasts. *Mol. Cell. Biol.* **15**, 1942-1952. doi:10.1128/MCB.15.4.1942
Kreis, S., Schonfeld, H. J., Melchior, C., Steiner, B. and Kieffer, N. (2005). The intermediate filament protein vimentin binds specifically to a recombinant integrin alpha2/beta1 cytoplasmic tail complex and co-localizes with native alpha2/beta1 in endothelial cell focal adhesions. *Exp. Cell Res.* **305**, 110-121. doi:10.1016/j.yexcr.2004.12.023
Lamouille, S., Xu, J. and Derynck, R. (2014). Molecular mechanisms of epithelial-mesenchymal transition. *Nat. Rev. Mol. Cell Biol.* **15**, 178-196. doi:10.1038/nrm3758
Lee, W., Sodek, J. and McCulloch, C. A. (1996). Role of integrins in regulation of collagen phagocytosis by human fibroblasts. *J. Cell. Physiol.* **168**, 695-704. doi:10.1002/(SICI)1097-4652(199609)168:3<695::AID-JCP22>3.0.CO;2-X
Lenter, M., Uhlig, H., Hamann, A., Jeno, P., Imhof, B. and Vestweber, D. (1993). A monoclonal antibody against an activation epitope on mouse integrin chain beta 1 blocks adhesion of lymphocytes to the endothelial integrin alpha 6 beta 1. *Proc. Natl. Acad. Sci. USA* **90**, 9051-9055. doi:10.1073/pnas.90.19.9051
Li, Q. F., Spinelli, A. M., Wang, R., Anfinogenova, Y., Singer, H. A. and Tang, D. D. (2006). Critical role of vimentin phosphorylation at Ser-56 by p21-activated kinase in vimentin cytoskeleton signaling. *J. Biol. Chem.* **281**, 34716-34724. doi:10.1074/jbc.M607715200
Liao, Y. F., Gotwals, P. J., Koteliansky, V. E., Sheppard, D. and Van De Water, L. (2002). The EIIIA segment of fibronectin is a ligand for integrins alpha 9beta 1 and alpha 4beta 1 providing a novel mechanism for regulating cell adhesion by alternative splicing. *J. Biol. Chem.* **277**, 14467-14474. doi:10.1074/jbc.M201100200
Liu, C. Y., Lin, H. H., Tang, M. J. and Wang, Y. K. (2015a). Vimentin contributes to epithelial-mesenchymal transition cancer cell mechanics by mediating cytoskeletal organization and focal adhesion maturation. *Oncotarget* **6**, 15966-15983. doi:10.18632/oncotarget.3862
Liu, J., Wang, Y., Goh, W. I., Goh, H., Baird, M. A., Ruehland, S., Teo, S., Bate, N., Critchley, D. R., Davidson, M. W. et al. (2015b). Talin determines the nanoscale architecture of focal adhesions. *Proc. Natl. Acad. Sci. USA* **112**, E4864-E4873. doi:10.1073/pnas.1512025112
Lowery, J., Kuczmarski, E. R., Herrmann, H. and Goldman, R. D. (2015). Intermediate filaments play a pivotal role in regulating cell architecture and function. *J. Biol. Chem.* **290**, 17145-17153. doi:10.1074/jbc.R115.640359
Maemura, M., Akiyama, S. K., Woods, V. L., Jr and Dickson, R. B. (1995). Expression and ligand binding of alpha 2 beta 1 integrin on breast carcinoma cells. *Clin. Exp. Metastasis* **13**, 223-235. doi:10.1007/BF00133478
Mendez, M. G., Kojima, S. and Goldman, R. D. (2010). Vimentin induces changes in cell shape, motility, and adhesion during the epithelial to mesenchymal transition. *FASEB J.* **24**, 1838-1851. doi:10.1096/fj.09-151639
Menko, A. S., Bleaken, B. M., Libowitz, A. A., Zhang, L., Stepp, M. A. and Walker, J. L. (2014). A central role for vimentin in regulating repair function during healing of the lens epithelium. *Mol. Biol. Cell* **25**, 776-790. doi:10.1091/mbc.e12-12-0900
Nayal, A., Webb, D. J., Brown, C. M., Schaefer, E. M., Vicente-Manzanares, M. and Horwitz, A. R. (2006). Paxillin phosphorylation at Ser273 localizes a GIT1-PIX-PAK complex and regulates adhesion and protrusion dynamics. *J. Cell Biol.* **173**, 587-589. doi:10.1083/jcb.200509075
Nieto, M. A. (2009). Epithelial-mesenchymal transitions in development and disease: old views and new perspectives. *Int. J. Dev. Biol.* **53**, 1541-1547. doi:10.1387/ijdb.072410mn
Nobes, C. D. and Hall, A. (1999). Rho GTPases control polarity, protrusion, and adhesion during cell movement. *J. Cell Biol.* **144**, 1235-1244. doi:10.1083/jcb.144.6.1235
Pankov, R. and Yamada, K. M. (2002). Fibronectin at a glance. *J. Cell Sci.* **115**, 3861-3863. doi:10.1242/jcs.00059
Patteson, A. E., Pogoda, K., Byfield, F. J., Mandal, K., Ostrowska-Podhorodecka, Z., Charrier, E. E., Galie, P. A., Deptula, P., Bucki, R., McCulloch, C. A. et al. (2019). Loss of vimentin enhances cell motility through small confining spaces. *Small* **15**, e1903180. doi:10.1002/smll.201903180
Pinon, P., Pärssinen, J., Vazquez, P., Bachmann, M., Rahikainen, R., Jacquier, M.-C., Azizi, L., Määttä, J. A., Bastmeyer, M., Hytönen, V. P. et al. (2014). Talin-bound NPLY motif recruits integrin-signaling adapters to regulate cell spreading and mechanosensing. *J. Cell Biol.* **205**, 265-281. doi:10.1083/jcb.201308136
Pinto, V. I., Mohammadi, H., Lee, W. S., Cheung, A. H. and McCulloch, C. A. (2015). PAK1 is involved in sensing the orientation of collagen stiffness gradients in mouse fibroblasts. *Biochim. Biophys. Acta* **1853**, 2526-2538. doi:10.1016/j.bbamcr.2015.05.019
Pirruccello, M., Sondermann, H., Pelton, J. G., Pellicena, P., Hoelz, A., Chernoff, J., Wemmer, D. E. and Kuriyan, J. (2006). A dimeric kinase assembly underlying autophosphorylation in the p21 activated kinases. *J. Mol. Biol.* **361**, 312-326. doi:10.1016/j.jmb.2006.06.017
Puklin-Faucher, E. and Sheetz, M. P. (2009). The mechanical integrin cycle. *J. Cell Sci.* **122**, 179-186. doi:10.1242/jcs.042127
Rane, C. K. and Minden, A. (2014). P21 activated kinases: structure, regulation, and functions. *Small GTPases* **5**, e28003. doi:10.4161/sgtp.28003
Rudolph, J., Crawford, J. J., Hoeflich, K. P. and Chernoff, J. (2013). p21-activated kinase inhibitors. *Enzymes* **34**, 157-180. doi:10.1016/B978-0-12-420146-0.00007-X
Schoumacher, M., Goldman, R. D., Louvard, D. and Vignjevic, D. M. (2010). Actin, microtubules, and vimentin intermediate filaments cooperate for elongation of invadopodia. *J. Cell Biol.* **189**, 541-556. doi:10.1083/jcb.200909113
Segal, G., Lee, W., Arora, P. D., McKee, M., Downey, G. and McCulloch, C. A. (2001). Involvement of actin filaments and integrins in the binding step in collagen phagocytosis by human fibroblasts. *J. Cell Sci.* **114**, 119-129.
Shattil, S. J., Kim, C. and Ginsberg, M. H. (2010). The final steps of integrin activation: the end game. *Nat. Rev. Mol. Cell Biol.* **11**, 288-300. doi:10.1038/nrm2871
Shi, A. M., Tao, Z. Q., Li, R., Wang, Y. Q., Wang, X. and Zhao, J. (2016). Vimentin and post-translational modifications in cell motility during cancer - a review. *Eur. Rev. Med. Pharmacol. Sci.* **20**, 2603-2606.
Shibue, T. and Weinberg, R. A. (2017). EMT, CSCs, and drug resistance: the mechanistic link and clinical implications. *Nat. Rev. Clin. Oncol.* **14**, 611-629. doi:10.1038/nrclinonc.2017.44
Snider, N. T. and Omary, M. B. (2014). Post-translational modifications of intermediate filament proteins: mechanisms and functions. *Nat. Rev. Mol. Cell Biol.* **15**, 163-177. doi:10.1038/nrm3753
Stone, R. C., Pastar, I., Ojeh, N., Chen, V., Liu, S., Garzon, K. I. and Tomic-Canic, M. (2016). Epithelial-mesenchymal transition in tissue repair and fibrosis. *Cell Tissue Res.* **365**, 495-506. doi:10.1007/s00441-016-2464-0
Tanentzapf, G. and Brown, N. H. (2006). An interaction between integrin and the talin FERM domain mediates integrin activation but not linkage to the cytoskeleton. *Nat. Cell Biol.* **8**, 601-606. doi:10.1038/ncb1411
Terriac, E., Coceano, G., Mavajian, Z., Hageman, T. A., Christ, A. F., Testa, I., Lautenschlager, F. and Gad, A. K. (2017). Vimentin levels and serine 71 phosphorylation in the control of cell-matrix adhesions, migration speed, and shape of transformed human fibroblasts. *Cells* **6**, 2. doi:10.3390/cells6010002
Thiery, J. P. and Sleeman, J. P. (2006). Complex networks orchestrate epithelial-mesenchymal transitions. *Nat. Rev. Mol. Cell Biol.* **7**, 131-142. doi:10.1038/nrm1835
Thiery, J. P., Acloque, H., Huang, R. Y. and Nieto, M. A. (2009). Epithelial-mesenchymal transitions in development and disease. *Cell* **139**, 871-890. doi:10.1016/j.cell.2009.11.007
Tsuruta, D. and Jones, J. C. (2003). The vimentin cytoskeleton regulates focal contact size and adhesion of endothelial cells subjected to shear stress. *J. Cell Sci.* **116**, 4977-4984. doi:10.1242/jcs.00823
Uynuk-Ool, T., Rothdiener, M., Walters, B., Hegemann, M., Palm, J., Nguyen, P., Seeger, T., Stockle, U., Stegemann, J. P., Aicher, W. K. et al. (2017). The geometrical shape of mesenchymal stromal cells measured by quantitative shape descriptors is determined by the stiffness of the biomaterial and by cyclic tensile forces. *J. Tissue Eng. Regen. Med.* **11**, 3508-3522. doi:10.1002/term.2263
Venkov, C. D., Link, A. J., Jennings, J. L., Plieth, D., Inoue, T., Nagai, K., Xu, C., Dimitrova, Y. N., Rauscher, F. J. and Neilson, E. G. (2007). A proximal activator of transcription in epithelial-mesenchymal transition. *J. Clin. Invest.* **117**, 482-491. doi:10.1172/JCI29544
Vohnoutka, R. B., Gulvady, A. C., Goreczny, G., Alpha, K., Handelman, S. K., Sexton, J. Z. and Turner, C. E. (2019). The focal adhesion scaffold protein Hic-5 regulates vimentin organization in fibroblasts. *Mol. Biol. Cell* **30**, 3037-3056. doi:10.1091/mbc.E19-08-0442
Wang, J., Su, Y., Iacob, R. E., Engen, J. R. and Springer, T. A. (2019). General structural features that regulate integrin affinity revealed by atypical alphaVbeta8. *Nat. Commun.* **10**, 5481. doi:10.1038/s41467-019-13248-5
Wang, Q., Rajshankar, D., Branch, D. R., Siminovitch, K. A., Herrera Abreu, M. T., Downey, G. P. and McCulloch, C. A. (2009). Protein-tyrosine phosphatase-alpha and Src functionally link focal adhesions to the endoplasmic reticulum to mediate interleukin-1-induced Ca^{2+} signaling. *J. Biol. Chem.* **284**, 20763-20772. doi:10.1074/jbc.M808828200
Welf, E. S., Naik, U. P. and Ogunnaike, B. A. (2012). A spatial model for integrin clustering as a result of feedback between integrin activation and integrin binding. *Biophys. J.* **103**, 1379-1389. doi:10.1016/j.bpj.2012.08.021

Winograd-Katz, S. E., Fassler, R., Geiger, B. and Legate, K. R. (2014). The integrin adhesome: from genes and proteins to human disease. *Nat. Rev. Mol. Cell Biol.* **15**, 273-288. doi:10.1038/nrm3769

Zeltz, C. and Gullberg, D. (2016). The integrin-collagen connection–a glue for tissue repair? *J. Cell Sci.* **129**, 653-664. doi:10.1242/jcs.180992

Zhao, Z. S. and Manser, E. (2012). PAK family kinases: physiological roles and regulation. *Cell Logist* **2**, 59-68. doi:10.4161/cl.21912

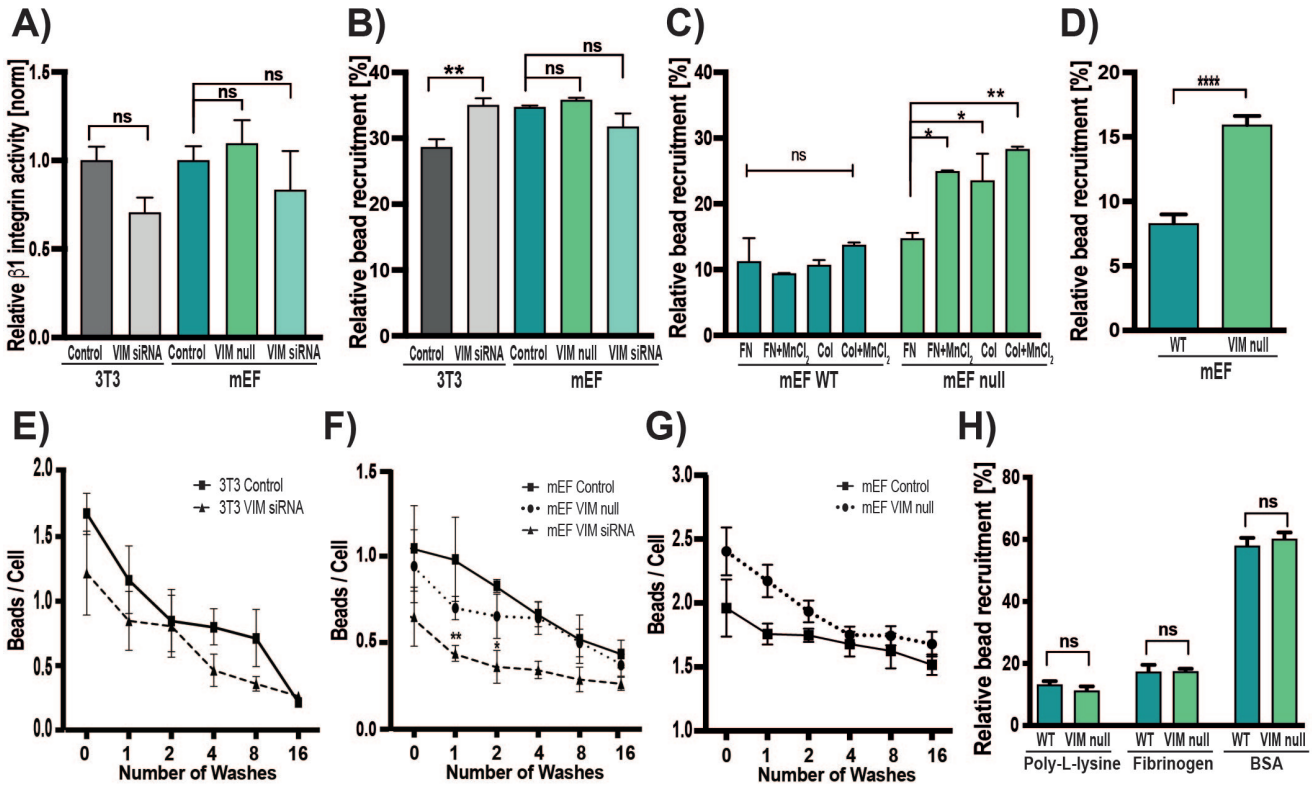

Fig. S1. (A) Estimation of relative β1 integrin activation levels after 3h incubation on fibronectin-coated tissue culture dishes. Cells were immunostained for β1 integrin with 9EG7 clone antibody. (B) Histogram shows relative recruitment of fibronectin-coated 2 μm fluorescent beads for all indicated cell types from flow cytometry analyses. 3T3 control cells (dark gray) and Vim siRNA (light gray), mEF control (teal), mEF Vim null (green) and mEF Vim siRNA (turquoise). (C) Recruitment of fibronectin or collagen-coated beads for mEF WT and Vim null cells after β1 integrin activation by 0.2 mM $MnCl_2$. (D) Quantification of fibronectin-coated beads recruitment by mEF WT and null plated on 0.01 mg/ml fibronectin-coated dishes. Quantification of the relative binding strength of control cells (square, solid line) and vimentin-depletion (Vim siRNA - triangle, dashed line; Vim null- circle, dotted line) 3T3 (E) and mEF cells (F). Fluorescent beads (2 μm) were coated with 1 mg/ml fibronectin and incubated with cells (8 beads/cell) for 2h. (G) Fibronectin-coated beads binding strength for mEF WT (square, solid line) and null (circle, dotted line) cells plated on 0.01 mg/ml fibronectin-coated dishes. Cells with bounded beads were subjected to 0, 1, 2, 4, 8, and 16 washes. Plots represent the number of bounded beads per cell after each wash. Quantification was done by ImageJ software. All data are reported as a mean ± S.E.M. Assessment of fluorescent beads recruitment by mEF WT and mEF null cells were done by flow cytometry. (H) Yellow-green (2 μm) beads were coated with poly-L-lysine, fibrinogen, or BSA, respectively. Quantification was done by FCS Express 6 software. All experiments were repeated four times, and data are reported as a mean ± S.E.M.

Fig. S2

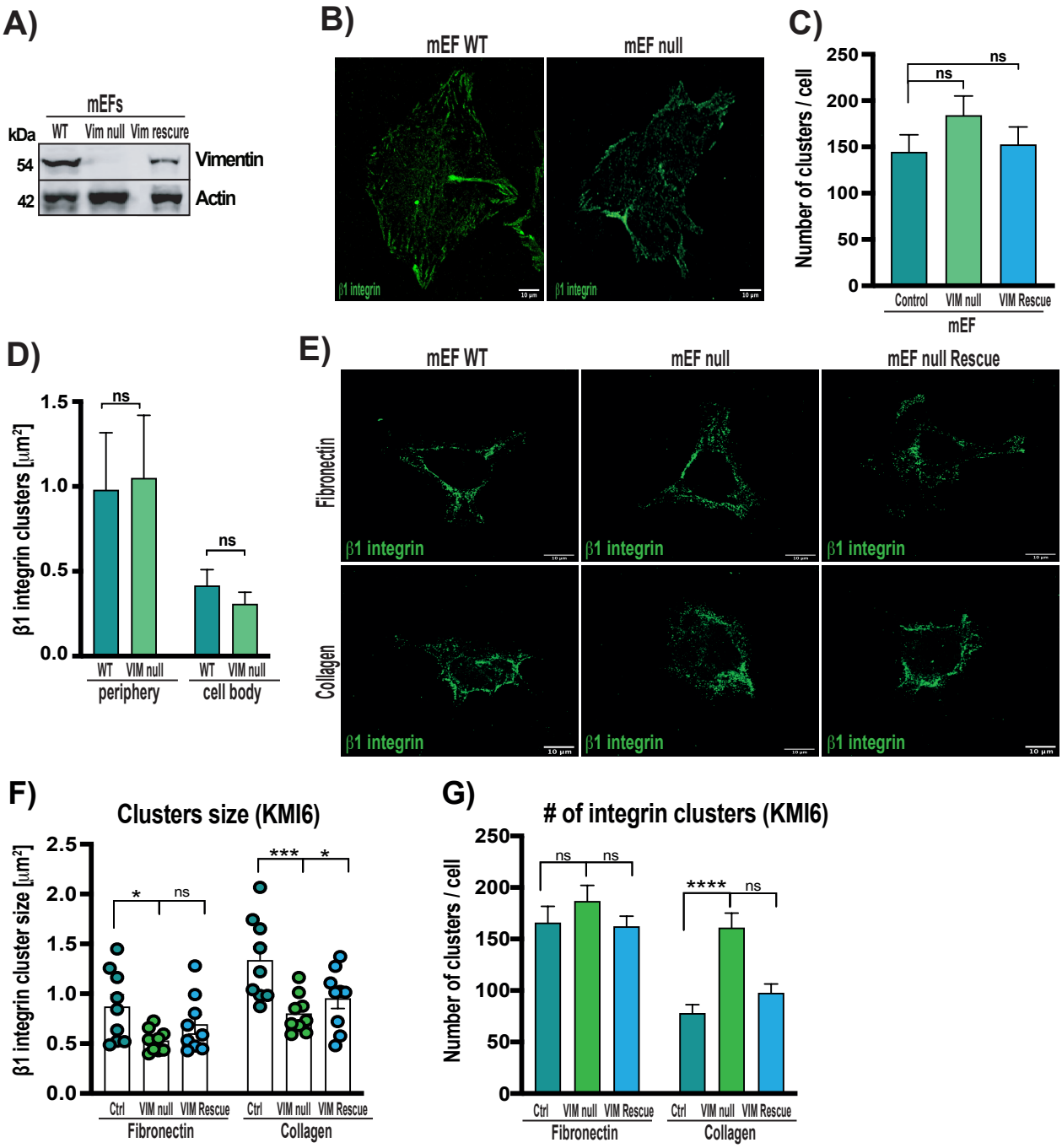

Fig. S2. (A) Western blot represents vimentin expression in mEF WT, mEF VIM rescue and mEF null cells. β-actin was used as a loading indicator. (B) Confocal images of β1 integrin in mEF WT and null cells plated on fibronectin-coated surfaces. Scale bar 10 μm. Quantification of β1 integrin cluster numbers (C) and cluster size (D) for mEF control (teal), mEF null (green), Vim rescue (blue). (E) Representative confocal images for mEF WT, Vim null and Vim rescue cells plated on fibronectin or collagen-coated surfaces staining for the total β1 integrin (KMI6 clone antibody). MEF control (teal), mEF Vim null (green) and mEF Vim siRNA (turquoise) and mEF Vim rescue cells (blue bars) were analyzed for: (F) β1 integrin cluster mean size (μm^2), and (G) β1 integrin cluster number per cell. All quantifications are from three experiments. *$p<0.05$, ****$p<0.0001$. All data are reported as a mean ± S.E.M, (n=3, at least 30 cells per group).

A)

2020 Scaffold Results from Orbitrap LC-MS					Abundance
Description	Accession	Number of Peptides	MW in kDa	Gene Symbol	Ratio mEF Null vs WT
Vimentin OS=Mus musculus (Mouse) OX=10090 GN=Vim PE=1 SV=3	**P20152**	**73**	**53.7**	**Vim**	**0.03**
Clathrin heavy chain 1 OS=Mus musculus (Mouse) OX=10090 GN=Cltc PE=1 SV=3	Q68FD5	52	191.4	Cltc	1.141
Alpha-actinin-1 OS=Mus musculus (Mouse) OX=10090 GN=Actn1 PE=1 SV=1	Q7TPR4	42	103	Actn1	1.405
Actin, cytoplasmic 1 OS=Mus musculus (Mouse) OX=10090 GN=Actb PE=1 SV=1	P60710	32	41.7	Actb	1.886
Collagen alpha-1(III) chain OS=Mus musculus (Mouse) OX=10090 GN=Col3a1 PE=1 SV=4	P08121	24	138.9	Col3a1	1.969
Talin-1 OS=Mus musculus (Mouse) OX=10090 GN=Tln1 PE=1 SV=2	**P26039**	**133**	**269.7**	**Tln1**	**2.491**
Integrin-linked protein kinase OS=Mus musculus (Mouse) OX=10090 GN=Ilk PE=1 SV=2	O55222	20	51.3	Ilk	2.636
Myosin regulatory light chain 12B OS=Mus musculus (Mouse) OX=10090 GN=Myl12b PE=1 SV=2	Q3THE2	12	19.8	Myl12b	2.97
Spectrin beta chain, non-erythrocytic 1 OS=Mus musculus (Mouse) OX=10090 GN=Sptbn1 PE=1 SV=2	Q62261	133	274.1	Sptbn1	3.722
Myosin-10 OS=Mus musculus (Mouse) OX=10090 GN=Myh10 PE=1 SV=2	Q61879	160	228.9	Myh10	4.103
Spectrin alpha chain, non-erythrocytic 1 OS=Mus musculus (Mouse) OX=10090 GN=Sptan1 PE=1 SV=4	P16546	166	284.4	Sptan1	4.525

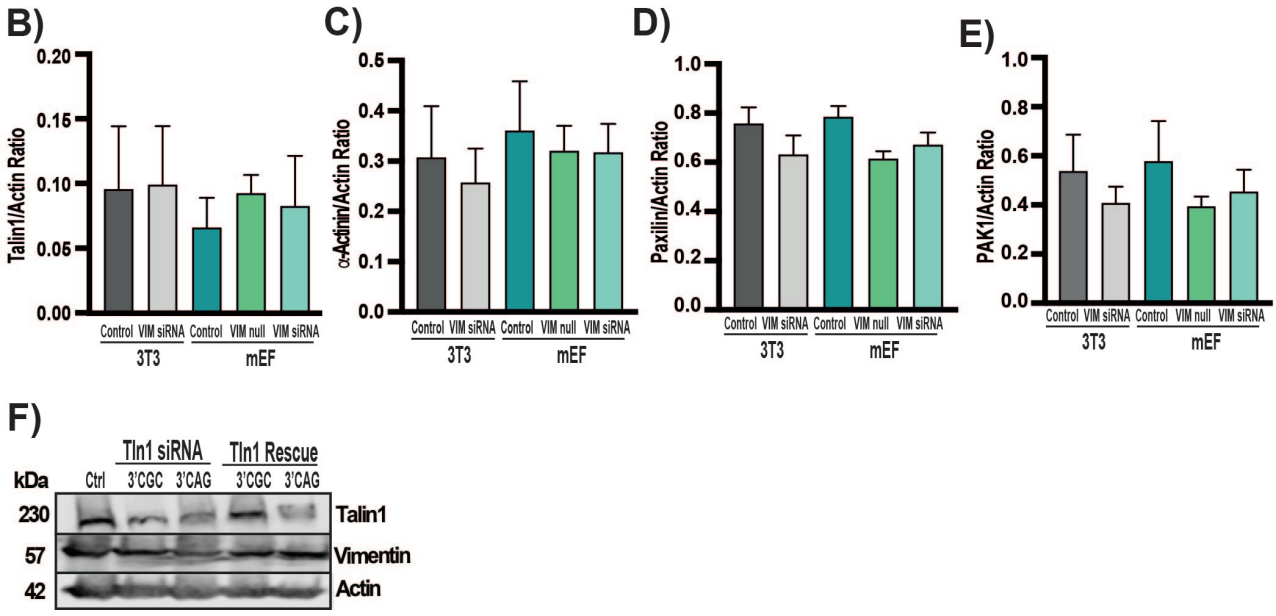

Fig. S3. (A) Mass spectrometry data of collagen bead-associated proteins analyzed presented as an abundance ratio for mEF WT and mEF null cells. Scaffold 4.10 (Proteome Software, Portland, OR, USA) was used for analyzing search results, calculating P values for each peptide match and matching peptide spectra. (B-E) Bar graphs represent talin:β-actin ratio (B); α-actinin:β-actin ratio (C); Paxillin:β-actin ratio (D) and PAK1:β-actin ratio (E) in the analyzed cell lines that were plated on fibronectin (black bars) or collagen (green bars) matrices. Quantifications were done based on western blot analysis (Fig. 4B) immunostained for talin, α-actinin, paxillin, PAK1 and β-actin (loading control) with appropriate antibodies. All data are reported as a mean ± S.E.M. (F) Immunoblotting represents Talin expression after 3'UTR CGC and CAG Tln siRNA and Tln re-expression (Tln-GFP plasmid), compared with control samples treated with scramble siRNA. Vimentin and β-actin were used as a loading control. All data are reported as a mean ± S.E.M, n=3.

Fig. S4

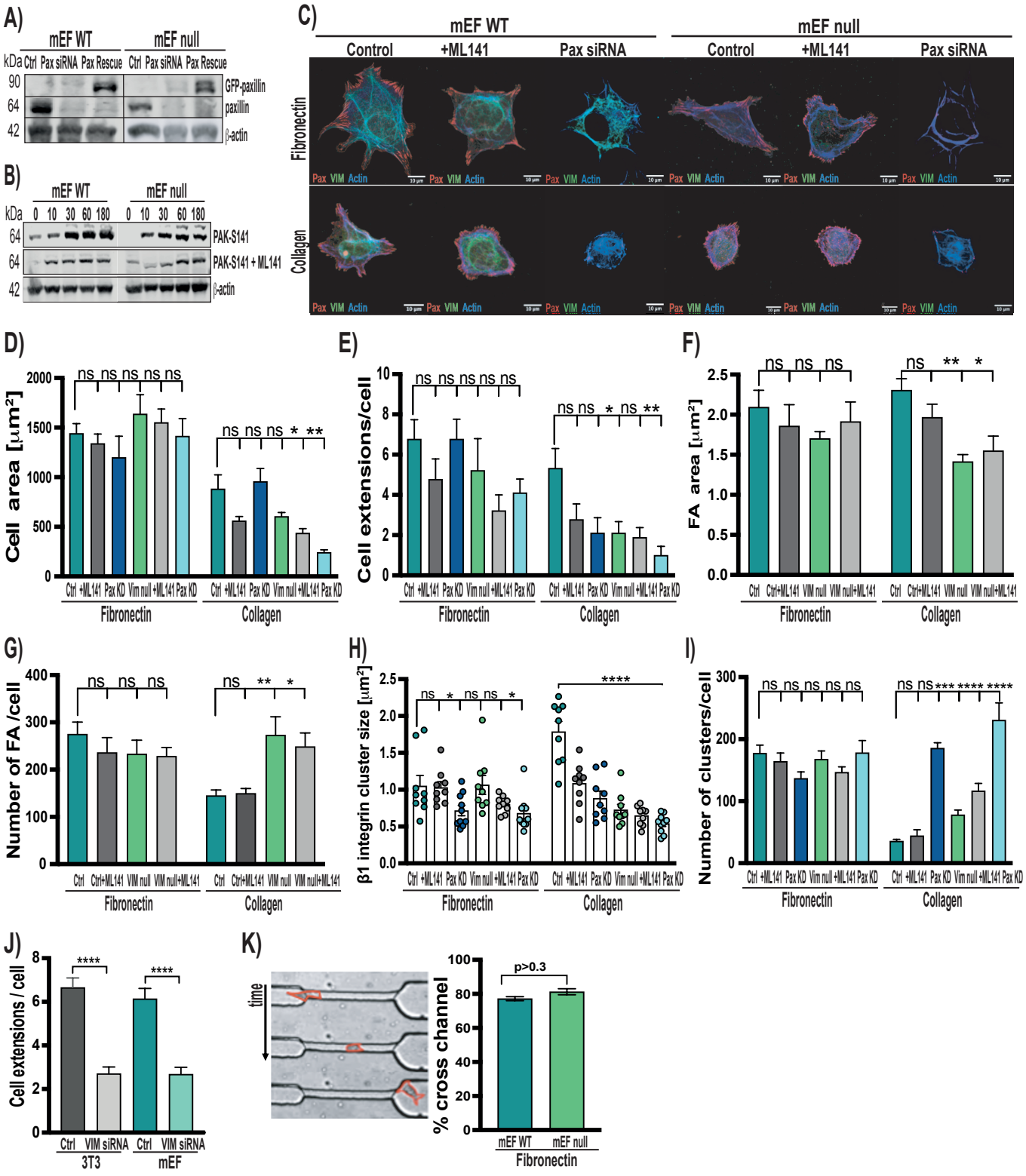

Fig. S4. Immunoblotting shows (A) paxillin (Pax) expression efficiency in vimentin WT and null mEFs. Cells were treated with scrambled siRNA (Ctrl), ON-TARGET paxillin siRNA (Pax siRNA) and paxillin-GFP plasmid. β-actin was used as a loading control. (B) mEFs were plated for the indicated times (0,10, 30, 60, and 180 min), lysed and immunoblotted for the indicated proteins, which include actin and PAK phospho-serine 141. The upper panel shows vehicle- treated samples (control). The middle panel shows cells treated with ML141, a specific Cdc42/Rac1 inhibitor (10 μM). Actin was used as a loading control. Experiments were performed in triplicates. All data are reported as a mean ± S.E.M, n=3. (C) Representative confocal images of mEFs treated with ML141 or paxillin siRNA cultured on fibronectin or collagen-coated surfaces and staining for paxillin (red), vimentin (green) and actin (blue). Scale bar 10 μm. Assessment cell morphology defined by (D) the mean area of cell and (E) the number of cells extensions per cell for mEF WT (control-teal), mEF WT+ML141 (dark gray bar), mEF Pax KD (dark blue), mEF null (green), mEF null+ML141 (light gray), mEF null Pax KD (light blue) plated on fibronectin or collagen-coated surfaces. Quantification of the focal adhesion size (F) and number (F) form mEF WT and null cells treated with 10 ⌈M ML141. Estimation of the β1 integrin cluster size (H) and average number (I) for mEF WT (control-teal), mEF WT+ML141 (dark gray bar), mEF Pax KD (dark blue), mEF null (green), mEF null +ML141 (light gray), mEF null Pax KD (light blue) plated on fibronectin or collagen-coated surfaces. (J) Number of cell protrusions per cell for 3T3 cells and mEFs after vimentin deletion and then cultured on fibronectin. All data are reported as a mean ± S.E.M, n=3. (K) Vimentin WT and null mEF migration through fibronectin-coated microchannel (at least 45 cells were counted; n=3). Experiment was conducted as described in (Patteson et al., 2019).

Fig. S5

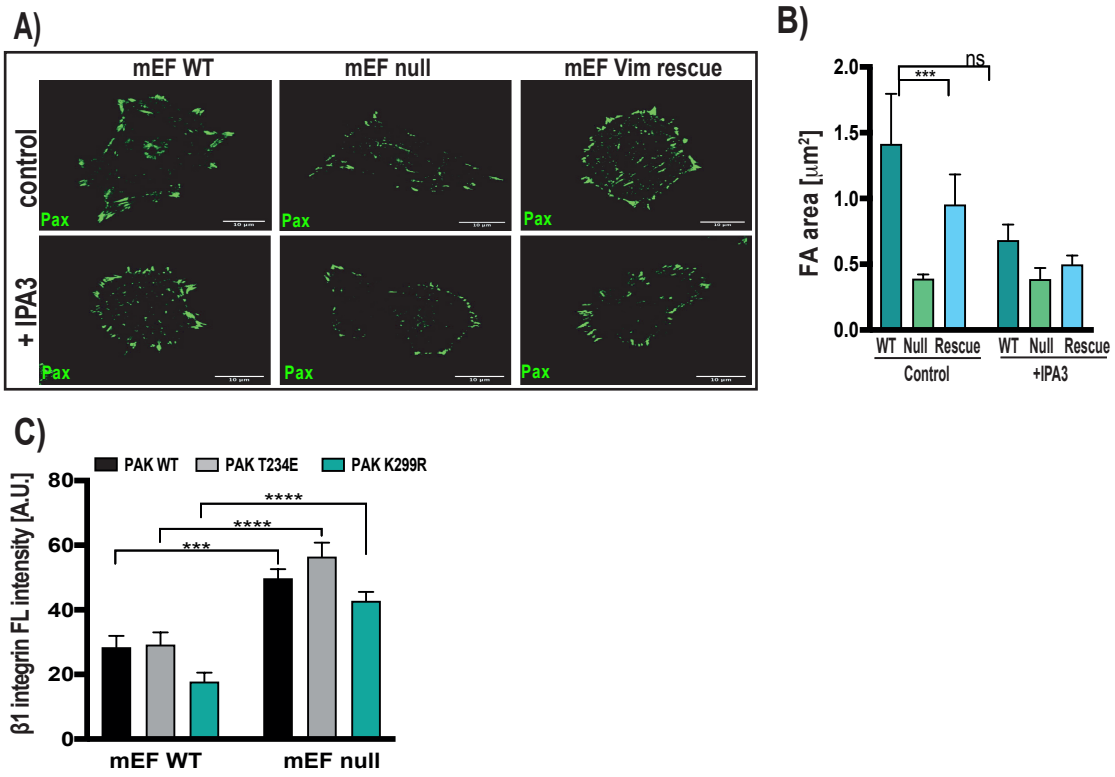

Fig. S5. Inhibition of PAK1 activity and vimentin expression alters focal adhesion size. (A) Representative fluorescence confocal images of cells treated with vehicle (control) or IPA3 (5 mM) and plated on collagen for 3h. Cells were fixed and immunostained with paxillin antibody (green). Scale bar, 10 μm. (B) Bar graphs represent size (μm^2) of focal adhesion in mEFs cells treatment with vehicle (control) and IPA3 (5 μM). MEF WT (tile bars), mEF null (green bars), and mEF VIM rescue (blue bars). Quantifications were done based on confocal images (Fig. 5A). (C) Impact of PAK1 kinase mutants on the β1 integrin activity for mEF WT and null cells. PAK1 WT (black), PAK1 constitutively active T423E (gray), PAK1 dominant negative mutant K299R (teal). Data are obtained from three independent experiments and reported as a mean ± S.E.M, *** $p<0.001$, **** $p<0.0001$.